ЖЭТФ, 1998, том 113, вып. 6, стр. 1930–1962

THE DIFFRACTION CONE FOR EXCLUSIVE VECTOR MESON PRODUCTION IN DEEP INELASTIC SCATTERING

J. Nemchik[a,b], *N. N. Nikolaev*[c,d], *E. Predazzi*[a], *B. G. Zakharov*[d], *V. R. Zoller*[e]

[a] *Dipartimento di Fisica Teorica, Università di Torino, and INFN, Sezione di Torino*
I-10125 Torino, Italy
[b] *Institute of Experimental Physics, Slovak Academy of Sciences*
04353 Košice, Slovak Republic
[c] *IKP(Theorie), KFA Jülich*
5170 Jülich, Germany
[d] *L. D. Landau Institute for Theoretical Physics, Russian Academy of Sciences*
117334, Moscow, Russia
[e] *Institute for Theoretical and Experimental Physics*
117218, Moscow, Russia

Submitted 25 December 1997

We develop the color dipole gBFKL phenomenology of a diffraction cone for photo- and electroproduction $\gamma^* N \to VN$ of heavy vector mesons (charmonium & bottonium) at HERA and in fixed target experiments. We predict a substantial shrinkage of the diffraction cone from the CERN/FNAL to the HERA range of c.m.s. energy W. The Q^2-controlled selectivity to the color dipole size (scanning phenomenon) is shown to lead to a decrease of the diffraction slope with Q^2 (which is supported by the available experimental data). We predict an approximate flavor independence of the diffraction slope in the scaling variable $Q^2 + m_V^2$. For diffractive production of the radially excited $2S$ states (Ψ', Υ'), the counterintuitive inequality of diffraction slopes $B(2S) \lesssim B(1S)$ is predicted, which defies the common wisdom that diffraction slopes are larger for reactions with larger size particles.

1. INTRODUCTION

Diffractive real and virtual photoproduction of ground state $V(1S)$ and radially excited $V'(2S)$ vector mesons,

$$\gamma^* p \to V(1S)p, V'(2S)p, \tag{1}$$

at high c.m.s. energy $W = \sqrt{s}$ is an ideal testing ground of ideas on the QCD pomeron exchange. The new experimental data on vector meson production coming from the HERA and fixed target experiments give a unique insight into how the pomeron exchange evolves from the nonperturbative to semiperturbative and to perturbative regimes with the increasing virtuality of the photon Q^2 and/or increasing mass m_V of the produced vector meson and have prompted intense theoretical discussions [1–11].

The usual approach to the perturbative QCD (pQCD) pomeron is based on the BFKL equation [12, 13] for the leading-log$s$ (LLs) evolution of the gluon distribution, formulated in the scaling approximation of fixed QCD coupling α_S = const and of infinite gluon correlation (propagation) radius R_c (massless gluons); it sums the ladder diagrams with reggeized t-channel gluon exchanges. More recently, a novel s-channel approach to the LLs BFKL equation has been developed [14, 15] in terms of the color dipole cross section $\sigma(\xi, r)$ (hereafter r is the

color dipole moment, $x_{eff} = (m_V^2 + Q^2)/(W^2 + Q^2)$ and $\xi = \log(1/x_{eff})$ is the rapidity variable). The color dipole approach, to be referred to as the running gBFKL approach, is favored because it incorporates consistently the two crucial properties of QCD: 1) asymptotic freedom (AF), i.e., the running QCD coupling $\alpha_S(r)$ and, 2) the finite propagation radius R_c of perturbative gluons. AF and the running $\alpha_S(r)$ are an indispensable feature of the modern theory of deep inelastic scattering (DIS); without running $\alpha_S(r)$ it is impossible to match the leading-$\log Q^2$ (LLQ^2) limit of the gBFKL equation with the conventional GLDAP equation [16] in the overlapping applicability region of the moderately small x ([14, 17], see also [13, 18, 19]). The finite R_c is of great importance since the nonperturbative fluctuations in the QCD vacuum restrict the phase space for the soft perturbative (real and virtual) gluons and there is a strong evidence for finite R_c from the lattice QCD studies (for the review see [20] and references therein) and hadronic interactions [21, 22]. In the infrared region, one also needs to freeze $\alpha_S(r)$ in order not to run into the Landau pole, $\alpha_S(r) \leq \alpha_S^{(fr)}$. Of course, if in our running gBFKL equation [14, 15] one puts $R_c = \infty$ and $\alpha_S = \text{const}$, then the original scaling BFKL equation [12, 13] is recovered [17, 23].

Being formulated in terms of real (rather than reggeized) gluon exchanges, the color dipole running gBFKL equation [14, 15] readily incorporates the running $\alpha_S(r)$. The effect of finite R_c can be including by modifying the gluon propagator in the infrared region, for instance, introducing the effective gluon mass $\mu_g \approx 1/R_c$. Remarkably, in LLs approximation, a finite R_c is consistent with QCD gauge invariance. The freezing of $\alpha_S(r)$ and the gluon correlation radius R_c are the nonperturbative parameters which describe the transition from the soft, infrared, to the perturbative, hard, region. The purely perturbative pomeron exchange does not exhaust the scattering amplitude and in the practical phenomenology of deep inelastic scattering one must add certain soft nonperturbative exchange. It is important that the color dipole picture and color dipole factorization for the proton structure function and for exclusive diffractive amplitudes do not require the validity of pQCD and are viable also for the soft pomeron exchange. The soft pomeron exchange is important only for sufficiently large color dipoles, $r > R_c$, and can readily be extracted from the experimental data on hadronic cross sections [24] and diffractive leptoproduction of light vector mesons [9]. On the other hand, the pQCD, or hard, pomeron exchange can be related to the perturbative gluon structure function of the proton [14, 25].

Diffractive production of $V(1S)$ mesons is particularly interesting because of the so-called scanning phenomenon, by which the production amplitude probes the color dipole cross section at the dipole size $r \sim r_S$, where

$$r_S \approx \frac{A}{\sqrt{Q^2 + m_V^2}}, \tag{2}$$

is the scanning radius [3–5]. This scanning property follows from the color dipole factorization for production amplitudes and the shrinkage of the transverse size of the virtual photon with Q^2 and holds beyond the pQCD domain [24]. Varying Q^2 one can study the transition from large, nonperturbative and semiperturbative, dipole size r_S to the perturbative region of very short $r_S \ll R_c$ in a very well controlled fashion [9, 10]. Furthermore, the scanning radius r_S defines the transverse size of the $\gamma^* V$ transition vertex, which contributes to the total interaction radius and to the diffraction slope $B(\gamma^* \to V)$. Motivated by a remarkable phenomenological success of such a unified color dipole picture of hard and soft pomeron in application to the proton structure function [26, 27] and vector meson production [5, 10], in this communication we develop the color dipole description of the forward diffraction cone $B(\gamma^* \to V)$ in exclusive

diffractive DIS. We use our early results for the energy dependence of the forward cone in color dipole scattering [28], obtained from the solution of the running gBFKL equation for the diffraction slope [29]. Here the crucial point is that breaking of the scale invariance by AF, i.e., by running $\alpha_S(r)$, and finite R_c, alters dramatically the very nature of the BFKL pomeron from a fixed cut in the scaling approximation to a series of moving poles for the running gBFKL pomeron [29, 27] (for early quasiclassical analysis see also [13]). As a result, in the running gBFKL approach one predicts a substantial Regge shrinkage of the diffraction slope in the vector meson production, which can be tested at HERA. In this paper we present for the first time the detailed analysis of the Q^2 dependence and of the Regge growth of the diffraction slope for the production of charmonium and bottonium states.

Diffractive production of radially excited $V'(2S)$ mesons will give an additional insight into the dipole size dependence of the diffraction slope. Because of the node in the radial wave function of the $V'(2S)$ states, there is a strong cancellation between contributions to the production amplitude from dipoles r larger than or smaller than the node position r_n (the node effect [1, 3, 30]). The resulting strong suppression of diffractive production of $V'(2S)$ vs. $V(1S)$ has been confirmed experimentally in the J/Ψ and Ψ' photoproduction at HERA and in fixed target experiments [31–33]. It has also interesting manifestations in the differential cross sections, which we discuss in the present paper for the first time. Because the radius of the $V'(2S)$ state is larger than the radius of the ground state $V(1S)$, for the diffraction slopes one would naively expect the inequality $B(\gamma^* \to \Psi') > B(\gamma^* \to J/\Psi)$. However, in this paper we demonstrate that the node effect in conjunction with the color dipole factorization predicts a counterintuitive inequality $B(\gamma^* \to \Psi') \lesssim B(\gamma^* \to J/\Psi)$, which can be tested at HERA. Because the node effect is sensitive to the form of the dipole cross section and its variation with energy, we predict specific energy dependence of the $V'(2S)/V(1S)$ production ratios, which also can be tested at HERA.

The presentation is organized as follows. The subject of the introductory Sec. 2 is the color dipole factorization and the determination of the pQCD factorization scales for diffractive production. The running gBFKL formalism for the calculation of the color dipole scattering matrix and of the diffraction slope is presented in Sec. 3. The decomposition of the diffraction slope into the perturbative and nonperturbative components and on what physics controls the W^2, flavor, and Q^2 dependence of the diffraction slope is expounded in Sec. 4. In Sec. 5 we discuss in more detail properties of the soft pomeron exchange in the color dipole representation. In Sec. 6 we present the salient features of the soft and hard exchanges on an example of VN total cross sections. Predictions from the running gBFKL dynamics for the forward and t-integrated vector mesons production cross section are reported in Sec. 7. We find a good agreement with the low energy data and the data from the HERA collider experiments. The subject of Sec. 8 is predictions for forward cone in diffractive production of $V(1S)$ states with special emphasis on flavor symmetry. Section 9 is concerned with the node effect in forward production of $V(2S)$ states. The summary and some conclusions are presented in Sec. 10.

2. INTRODUCTION INTO COLOR DIPOLE FACTORIZATION AND pQCD FACTORIZATION SCALES FOR DIFFRACTIVE AMPLITUDES

The Fock state expansion for the lightcone meson starts with the $q\bar{q}$ state; the snapshot of the relativistic meson as a $q\bar{q}$ color dipole. The probability amplitude to find the $q\bar{q}$ color dipole of size $\vec{r}$ is precisely the $q\bar{q}$ wave function, $\Psi(\vec{r}, z)$, where z is the fraction of meson's

lightcone momentum carried by a quark (the Sudakov lightcone variable). The interaction of the relativistic color dipole of the dipole moment $\vec{r}$ with the target nucleon is quantified by the energy dependent color dipole cross section, $\sigma(\xi, r)$. The effect of higher Fock states $q\bar{q}g...$ is very important at high energy ν. To the LLs and/or LL$1/x$ approximation it can be reabsorbed into the energy (rapidity) dependence of $\sigma(\xi, r)$, which is described by the running gBFKL equation [14, 15]. The dipole cross section is flavor independent and provides a unified description of various diffractive processes.

In the limit of high photon energy ν, the $q\bar{q}$-nucleon scattering matrix $\tilde{\mathcal{M}}$ becomes diagonal in the mixed $(\vec{r}, z)$-representation. This $(\vec{r}, z)$ diagonalization derives from the large longitudinal coherence length,

$$l_{coh} \sim \frac{2\nu}{Q^2 + m_V^2}, \tag{3}$$

and holds if $l_{coh} \gg R_p$, where R_p is a size of the target proton. Because the coherence length is a purely kinematical scale [34], the $(\vec{r}, z)$ diagonalization does not require the applicability of pQCD and must hold also for soft pomeron exchange, i.e. even if the dipole size $\vec{r}$ is large. The necessary condition is that the longitudinal scale l_{soft} for the soft pomeron exchange is small, $l_{soft} \ll l_{coh}$, which is the case for instance in the dual parton string model [35] or different models of exchange by nonperturbative gluons [36, 37, 11]. For the phenomenological success of a unified color dipole picture of vector meson production see [9, 10].

Taking advantage of the $(\vec{r}, z)$ diagonalization of the scattering matrix $\tilde{\mathcal{M}}$, the amplitude for real (virtual) photoproduction of vector mesons with the momentum transfer $\vec{q}$ can be represented in the color dipole factorized form

$$\mathcal{M}(\gamma^* \to V, \xi, Q^2, \vec{q}) = \langle V|\tilde{\mathcal{M}}|\gamma^*\rangle = \int_0^1 dz \int d^2r \Psi_V^*(\vec{r}, z)\mathcal{M}(\xi, r, z, \vec{q})\Psi_{\gamma^*}(\vec{r}, z). \tag{4}$$

Our normalization is such that $(d\sigma/dt)_{t=0} = |\mathcal{M}|^2/16\pi$. In Eq. (4), $\Psi_{\gamma^*}(\vec{r}, z)$ and $\Psi_V(\vec{r}, z)$ represent the probability amplitudes to find the color dipole of size $\vec{r}$ in the photon and quarkonium (vector meson), respectively (for the sake of brevity we suppress the spin indices), and $\mathcal{M}(\xi, r, z, \vec{q})$ is an amplitude for elastic scattering of the color dipole on the target nucleon. The color dipole distribution in (virtual) photons was derived in [24, 14].

The color dipole cross section $\sigma(\xi, r)$ only depends on the dipole size r but not on the q-$\bar{q}$ momentum partition z. Because in the nonrelativistic heavy quarkonium $z \approx 1/2$, at small $\vec{q}$ in the diffraction cone one can safely neglect the z-dependence of $\tilde{\mathcal{M}}$ and set $z = 1/2$. Hereafter we will suppress the argument z. Either ξ or x_{eff} will be used whenever convenient. (We notice that the straightforward analysis of the relevant Sudakov variables gives the relationship $x_{eff} \approx x$, where x is the Bjorken variable for the inclusive DIS.)

We focus on calculating the imaginary part of the scattering amplitude for which there is a simple representation in terms of the gluon density matrix (see below). The small real part can easily be reconstructed from analyticity considerations [38]

$$\mathrm{Re}\,\mathcal{M}(\xi, r, \vec{q}) = \frac{\pi}{2}\frac{\partial}{\partial \xi}\mathrm{Im}\,\mathcal{M}(\xi, r, \vec{q}). \tag{5}$$

We suppress the discussion of $\mathrm{Re}\,\mathcal{M}$, which is consistently included in all numerical results.

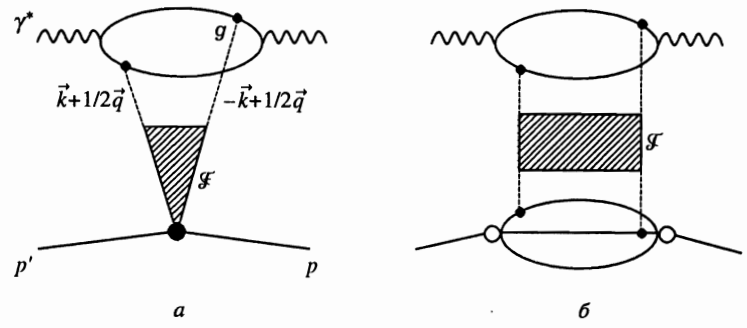

Fig. 1. The perturbative QCD diagrams for vector meson production

The details of calculation of the diffractive amplitude have been presented elsewhere [5, 10]. For the $Vq\bar{q}$ vertex function we assume the Lorentz structure $\Gamma\bar{\Psi}\gamma_\mu\Psi V_\mu$. For the s-channel helicity conservation at small $\vec{q}$, transversely (T) polarized photons produce the transversely polarized vector mesons and the longitudinally (L) polarized photons (to be more precise, scalar photons) produce longitudinally polarized vector mesons. One finds

$$\mathrm{Im}\,\mathcal{M}_T(x_{eff},Q^2,\vec{q}) = \frac{N_c C_V\sqrt{4\pi\alpha_{em}}}{(2\pi)^2}\times$$

$$\times\int d^2r\sigma(x_{eff},r,\vec{q})\int_0^1\frac{dz}{z(1-z)}\left\{m_q^2K_0(\varepsilon r)\phi(\vec{r},z)-\left[z^2+(1-z)^2\right]\varepsilon K_1(\varepsilon r)\partial_r\phi(\vec{r},z)\right\}, \quad (6)$$

$$\mathrm{Im}\,\mathcal{M}_L(x_{eff},Q^2,\vec{q}) = \frac{N_c C_V\sqrt{4\pi\alpha_{em}}}{(2\pi)^2}\,\frac{2\sqrt{Q^2}}{m_V}\times$$

$$\times\int d^2r\sigma(x_{eff},r,\vec{q})\int_0^1 dz\,K_0(\varepsilon r)\left\{\left[m_q^2+z(1-z)m_V^2\right]\phi(\vec{r},z)-\partial_r^2\phi(\vec{r},z)\right\}, \quad (7)$$

where

$$\varepsilon^2 = m_q^2 + z(1-z)Q^2\,, \quad (8)$$

α_{em} is the fine structure constant, $N_c = 3$ is the number of colors, $C_V = 1/\sqrt{2}$, $1/3\sqrt{2}$, 1/3, 2/3, 1/3 are the charge-isospin factors for the ρ^0, ω^0, ϕ^0, J/Ψ, and Υ production, respectively and $K_{0,1}(x)$ are the modified Bessel functions. The detailed discussion and parameterization of the lightcone radial wave function $\phi(r,z)$ of the $q\bar{q}$ Fock state of the vector meson are given in [10]. For heavy quarkonia one can safely identify the current and constituent quarks. The terms $\propto K_0(\varepsilon r)\phi(\vec{r},z)$ and $\propto \varepsilon K_1(\varepsilon r)\partial_r\phi(\vec{r},z)$ for T polarization, and $K_0(\varepsilon r)\partial_r^2\phi(\vec{r},z)$ for L polarization correspond to the helicity conserving and helicity-flip transitions in the $\gamma^*\to q\bar{q}$ and $V\to q\bar{q}$ vertices, respectively. In the nonrelativistic heavy quarkonia, the helicity flip transitions are the relativistic corrections, which become important only at large Q^2. Equation (7) corrects a slight mistake in the relativistic correction to the amplitude for production of longitudinally polarized photons made in [5]. The numerical results of Ref. 5 for the J/Ψ are only marginally different from those to be reported in this paper.

The representation for $\sigma(x,r,\vec{q})$ in terms of the gluon density matrix (see Fig. 1) is as follows:

$$\sigma(x,r,\vec{q}) = \frac{4\pi}{3}\int \frac{d^2k}{k^4}\,\alpha_S(\kappa^2)\left[J_0\left(\frac{1}{2}qr\right) - J_0(kr)\right]\mathscr{F}\left(x,\vec{k}+\frac{1}{2}\vec{q},-\vec{k}+\frac{1}{2}\vec{q}\right), \qquad (9)$$

where $J_0(x)$ is the usual Bessel function. AF dictates that at the gluon-color dipole vertex, the QCD running coupling must be taken at the largest relevant virtuality, $\kappa^2 = \max\{\vec{k}^2, C^2r^{-2}\}$, where $C \approx 1.5$ [24] and ensures the numerically similar results of calculations in both the mixed (r,z) and the momentum representations. The gluon density matrix $\mathscr{F}(x,\vec{k}+\vec{q}/2,-\vec{k}+\vec{q}/2)$ is proportional to the imaginary part of the nonforward gluon–nucleon scattering amplitude; at $\vec{q}=0$ it equals the unintegrated gluon structure function of the nucleon $\mathscr{F}(x,\vec{k},-\vec{k}) = \partial G(x,k^2)/\partial\log k^2$. Equation (9) generalizes to the nonforward case $\vec{q}\neq 0$ the formula [25, 14] for the dipole cross section

$$\sigma(x_{eff},r,\vec{q}=0) = \sigma(x_{eff},r) = \frac{\pi^2r^2}{3}\int \alpha_S(\kappa^2)\frac{dk^2}{k^2}\,\frac{4[1-J_0(kr)]}{(kr)^2}\,\frac{\partial G(x_{eff},k^2)}{\partial\log k^2}. \qquad (10)$$

Because the function $f(y) = 4[1-J_0(y)]/y^2$ can qualitatively be approximated by the step-function, $f(y)\approx\theta(A_\sigma - y)$, where $A_\sigma \approx 10$ [39], for small $r \ll R_c$ one readily finds

$$\sigma(x,r) = \frac{\pi^2}{3}r^2\alpha_s(r)G(x,q_\sigma^2), \qquad (11)$$

where the gluon structure function enters at the pQCD factorization scale $q_\sigma^2 \sim A_\sigma/r^2$ [14, 25, 39]. For large dipoles, $r \gtrsim R_c$, one can neglect $J_0(kr)$ in the integrand, and the dipole cross section saturates,

$$\sigma(x_{eff},r\gtrsim R_c) = \frac{4\pi^2}{3}\int \alpha_S(k^2)\frac{dk^2}{k^4}\,\frac{\partial G(x_{eff},k^2)}{\partial\log k^2}. \qquad (12)$$

Next, notice that the integrands in Eqs. (6) and (7) are smooth at small r and vanish exponentially at $r > 1/\varepsilon$ due to $K_{0,1}(\varepsilon r)$. Because of the behavior $\sigma(x,r)\propto r^2$ in (11), the amplitudes (6) and (7) are dominated by the contribution from the dipole size $r\approx r_S$ given by Eq. (2) — the scanning phenomenon [3–5]. The scanning property is best quantified in terms of the weight functions $W_{T,L}(Q^2,r^2)$ defined by

$$\mathscr{M}_T(x_{eff},Q^2,\vec{q}) = \frac{C_V}{(m_V^2+Q^2)^2}\int\frac{dr^2}{r^2}\,\frac{\sigma(x_{eff},r,\vec{q})}{r^2}W_T(Q^2,r^2), \qquad (13)$$

$$\mathscr{M}_L(x_{eff},Q^2,\vec{q}) = \frac{C_V}{(m_V^2+Q^2)^2}\,\frac{2\sqrt{Q^2}}{m_V}\int\frac{dr^2}{r^2}\,\frac{\sigma(x_{eff},r,\vec{q})}{r^2}W_L(Q^2,r^2), \qquad (14)$$

where in a somewhat abbreviated form ($i = T, L$, for the exact integrands see Eqs. (6) and (7))

$$W_i(Q^2,r^2) = \frac{\pi}{C_V}r^4(m_V^2+Q^2)^2\int_0^1 dz\Psi_{V_i}^*(r,z)\Psi_{\gamma_i^*}(r,z). \qquad (15)$$

For the $1S$ mesons to a good approximation the so-defined $W_{T,L}(Q^2,r^2)$ are sharply peaked functions of a natural variable $y = \log[r^2(Q^2+m_V^2)]$. The height and width of the peak

in y-distribution do only weakly vary with Q^2 and the flavor and the peak position defines the scanning radius $r_S \approx A_{T,L}/\sqrt{Q^2+m_V^2}$. Consequently, the leading twist terms in the expansion over the relevant short-distance parameter $r_S^2 \propto 1/(Q^2+m_V^2)$ are of the form (here we consider $\vec{q}=0$)

$$\mathrm{Im}\,\mathscr{M}_T \propto \frac{1}{Q^2+m_V^2}\sigma(x_{eff},r_S) \propto \frac{1}{(Q^2+m_V^2)^2}G(x_{eff},q_T^2)\,, \tag{16}$$

$$\mathrm{Im}\,\mathscr{M}_L \approx \frac{\sqrt{Q^2}}{m_V}\mathscr{M}_T \propto \frac{\sqrt{Q^2}}{m_V}\frac{1}{(Q^2+m_V^2)^2}G(x_{eff},q_L^2)\,. \tag{17}$$

By virtue of (11), here the pQCD scale $q_{T,L}^2 = \tau_{L,T}(Q^2+m_V^2)$, where the scale parameter $\tau_{T,L}$ can be estimated as

$$\tau_{T,L} \approx \frac{A_\sigma}{A_{T,L}^2}\,. \tag{18}$$

For the more direct evaluation of the pQCD factorization scales $q_{T,L}^2$ it is convenient to substitute Eq. (10) into (13) and (14), which then take the form reminiscent of the k-factorization formulas for $F_2(x,Q^2)$ [24, 40]:

$$\mathrm{Im}\,\mathscr{M}_T(x_{eff},Q^2,\vec{q}=0) = \frac{C_V\alpha_S(Q^2+m_V^2)}{(m_V^2+Q^2)^2}\int\frac{dk^2}{k^2}\frac{\partial G(x_{eff},k^2)}{\partial\log k^2}\Theta_T(Q^2,k^2), \tag{19}$$

$$\mathrm{Im}\,\mathscr{M}_L(x_{eff},Q^2,\vec{q}=0) = \frac{C_V\alpha_S(Q^2+m_V^2)}{(m_V^2+Q^2)^2}\frac{2\sqrt{Q^2}}{m_V}\int\frac{dk^2}{k^2}\frac{\partial G(x_{eff},k^2))}{\partial\log k^2}\Theta_L(Q^2,k^2), \tag{20}$$

where

$$\Theta_{T,L}(Q^2,k^2) = \frac{\pi^2}{3}\int\frac{dr^2}{r^2}\frac{\alpha_S(\kappa^2)}{\alpha_S(Q^2+m_V^2)}\frac{4[1-J_0(kr)]}{(kr)^2}W_{T,L}(Q^2,r^2)\,. \tag{21}$$

Because of properties of $f(y)$ and of the sharp peaking of $W_{T,L}(Q^2,r^2)$ at $r\approx r_S$, the weight functions $\Theta_{T,L}(Q^2,k^2)$ are similar to the step function,

$$\Theta_{T,L}(Q^2,k^2) \propto \theta(q_{T,L}^2-k^2)\,, \tag{22}$$

and

$$\int\frac{dk^2}{k^2}\frac{\partial G(x_{eff},k^2))}{\partial\log k^2}\Theta_i(Q^2,k^2) = G(x_{eff},q_i^2)\int\frac{dk^2}{k^2}\Theta_i(Q^2,k^2)) = G(x_{eff},q_i^2)I_i(Q^2)\,, \tag{23}$$

where the factors

$$I_{T,L}(Q^2) = \frac{\pi^2}{3}\int\frac{dr^2}{r^2}\frac{\alpha_S(\kappa^2)}{\alpha_S(Q^2+m_V^2)}W_{T,L}(Q^2,r^2) \tag{24}$$

exhibit only a marginal dependence on Q^2.

For small Q^2 the scale parameters $A_{T,L}$ are close to the nonrelativistic estimate $A\sim 6$, which follows from $r_S = 3/\varepsilon$ with the nonrelativistic choice $z=1/2$. In general, $A_{T,L}\geq 6$ and increase slowly with Q^2 [5]; for heavy quarkonia $A_{T,L}(\Upsilon)\simeq 6$ at $Q^2\leq 100$ GeV^2 and $A_{T,L}(J/\Psi)\sim 6$ at $Q^2=0$ and $A_{T,L}(J/\Psi)\simeq 7$ at $Q^2=100$ GeV^2, which shows the relativistic

corrections in the charmonium and bottonium electroproduction are small. The corollary of the large scanning radius r_S and large values of $A_{T,L}$ is a very small scale factor $\tau_{T,L}$ in the pQCD factorization scale [5]: $\tau_{T,L}(J/\Psi) \approx 0.20$, $\tau_L(\rho^0) \approx 0.15$ and $\tau_T(\rho^0) \approx 0.07$–$0.10$ for $Q^2 \sim 10$–100 GeV^2, which are substantially smaller than $\tau \approx 0.25$ suggested in [2] and $\tau \approx 1$ suggested in [6]. Consequently, the moderate values of Q^2 attainable at HERA do, at the best, correspond to the nonperturbative and semiperturbative values of $q^2_{T,L}$, the soft contribution to the vector meson production must be substantial and one must be careful with the interpretation of the vector meson production data in terms of the gluon structure function. The point that at $Q^2 \lesssim m^2_{J/\Psi}$ the scanning radius r_S is comparable to the radius of the J/Ψ, has been overlooked in [2] and the formulas of Ref. 2 for the J/Ψ production amplitudes in terms of the J/Ψ wave function at the origin are too crude. Strictly speaking, Eqs. (19), (20) and (23) were derived for the hard pQCD exchange when $r_S \lesssim R_c$ and/or for the perturbatively large $q^2_{T,L}$. However, because the color dipole factorization is true beyond pQCD, one can extend Eq. (10) to the soft pomeron and regard this relationship as an operational definition of the nonperturbative gluon distribution in the proton. To the same extent, Eqs. (19), (20), and (23) can serve as a unique basis for extracting the whole gluon distribution, perturbative plus nonperturbative, at small x from the experimental data on diffractive vector meson electroproduction at HERA.

The dominance of the longitudinal amplitude (17) at $Q^2 \gtrsim m^2_V$ follows, as a matter of fact, from electromagnetic gauge invariance and as such it is true in any reasonable model of vector meson production, the familiar vector dominance model (VDM) included. The Q^2 dependence of $\mathscr{M}_{T,L}$ differs drastically from the VDM prediction

$$\mathscr{M}_T(VDM) \propto \frac{1}{m_V^2 + Q^2}\sigma_{tot}(\rho N),$$

instead of $\sigma_{tot}(\rho N)$ in (16) one has $\sigma(x_{eff}, r_S) \propto r_S^2 \propto 1/(Q^2 + m_V^2)$.

3. THE DIFFRACTION CONE IN THE COLOR DIPOLE gBFKL APPROACH

In the familiar impact-parameter representation for amplitude of elastic scattering of the color dipole

$$\mathrm{Im}\,\mathscr{M}(\xi, r, \vec{q}) = 2\int d^2b\, \exp(-i\vec{q}\vec{b})\Gamma(\xi, \vec{r}, \vec{b}), \tag{25}$$

the diffraction slope $B = -2(d\log \mathrm{Im}\,\mathscr{M}/dq^2)_{q=0}$ equals

$$B(\xi, r) = \frac{1}{2}\langle \vec{b}^2 \rangle = \frac{\lambda(\xi, r)}{\sigma(\xi, r)}, \tag{26}$$

where

$$\lambda(\xi, r) = \int d^2b\, \vec{b}^2\, \Gamma(\xi, \vec{r}, \vec{b}). \tag{27}$$

Then, the generalization of the color dipole factorization formula (4) to the diffraction slope of the reaction $\gamma^* p \to Vp$ reads

$$B(\gamma^* \to V,\xi,Q^2)\,\mathrm{Im}\,\mathcal{M}(\gamma^* \to V,\xi,Q^2,\vec{q}=0) = \int_0^1 dz \int d^2r\lambda(\xi,r)\Psi_V^*(r,z)\Psi_{\gamma^*}(r,z)\,. \quad (28)$$

We sketch here the running gBFKL equation [28] for $\lambda(\xi,r)$. The running gBFKL equation for the energy dependence of the color dipole cross section reads [14, 15]

$$\frac{\partial\sigma(\xi,r)}{\partial\xi} = \mathscr{K}\otimes\sigma(\xi,r) = \frac{3}{8\pi^3}\times$$
$$\times\int d^2\rho_1\mu_G^2\left|g_S(R_1)K_1(\mu_G\rho_1)\frac{\vec{\rho}_1}{\rho_1} - g_S(R_2)K_1(\mu_G\rho_2)\frac{\vec{\rho}_2}{\rho_2}\right|^2[\sigma(\xi,\rho_1)+\sigma(\xi,\rho_2)-\sigma(\xi,r)]\,. \quad (29)$$

Here the kernel $\mathscr{K}$ is related to the wave function squared of the color-singlet $q\bar{q}g$ state with the Weizsäcker–Williams (WW) soft gluon, in which $\vec{r}$ is the $\bar{q}$-q separation and $\vec{\rho}_{1,2}$ are the q-g and $\bar{q}$-g separations in the two-dimensional impact parameter plane. The quantity

$$\vec{\mathscr{E}}(\vec{\rho}) = \mu_G g_S(\rho)K_1(\mu_G\rho)\frac{\vec{\rho}}{\rho} = -g_S(\rho)\nabla_\rho K_0(\mu_G\rho),$$

where $K_\nu(x)$ is the modified Bessel function, describes a Yukawa screened transverse chromoelectric field of the relativistic quark, and

$$\mu_G^2\left|g_S(R_1)K_1(\mu_G\rho_1)\frac{\vec{\rho}_1}{\rho_1} - g_S(R_2)K_1(\mu_G\rho_2)\frac{\vec{\rho}_2}{\rho_2}\right|^2 = \left|\vec{\mathscr{E}}(\vec{\rho}_1) - \vec{\mathscr{E}}(\vec{\rho}_2)\right|^2 \quad (30)$$

describes the flux (the modulus of the Poynting vector) of WW gluons in the $q\bar{q}g$ state. The asymptotic freedom of QCD uniquely prescribes the chromoelectric field be computed with the running QCD charge $g_S(r) = \sqrt{4\pi\alpha_S(r)}$ taken at the shortest relevant distance, $R_i = \min\{r,\rho_i\}$ in the $q\bar{q}g$ system. The particular combination of the three color dipole cross sections,

$$\Delta\sigma(\rho_1,\rho_2,r) = \frac{9}{8}\left[\sigma(\xi,\rho_1)+\sigma(\xi,\rho_2)-\sigma(\xi,r)\right], \quad (31)$$

which emerges in the r.h.s. of the gBFKL equation, is precisely a change of the color dipole cross section for the presence of the WW gluon [14] in the $q\bar{q}g$ state.

At short distances, $r,\rho_{1,2} \ll R_c = 1/\mu_G$, the kernel $\mathscr{K}$ does not depend on the infrared cutoff R_c. The Yukawa cutoff of the long range chromoelectric field which has been used in Eqs. (29) and (30) is the simplest phenomenological option. To the LL$(1/x)$ approximation, this cutoff is consistent with gauge invariance. If one sacrifices AF putting $g_S = \mathrm{const}$ and lifts the infrared cutoff by letting $R_c \to \infty$, one recovers the scale-invariant kernel $\mathscr{K}$. Both the finite R_c and running α_S break the scale invariance, the detailed discussion of consequences is found in [15, 17, 27, 29]. The principal phenomenon is that because of the lack of strong $\log r^2$ ordering in the BFKL equation there is an intrusion from hard scattering to the regime of soft interactions and vice versa, and the effect of the soft region is especially enhanced by AF. In the numerical analysis [15] an infrared freezing $\alpha_S(q^2) \le \alpha_S^{(fr)} = 0.82$ has been imposed on the three-flavor, one-loop $\alpha_S(q^2) = 4\pi/9\log(k^2/\Lambda^2)$ with $\Lambda = 0.3$ GeV. With $R_c = 0.27$ fm, i.e., $\mu_G = 0.75$ GeV, we found $\Delta_{\mathbf{P}} = 0.4$ [15], the calculation of Regge trajectories of subleading pomeron singularities is reported in [27], the emerging succesful description of the proton strcuture function at small x is published in [26, 27].

In [29] the gBFKL equation (29) has been generalized to the profile function $\Gamma(\xi,\vec{r},\vec{b})$, where the impact parameter $\vec{b}$ is defined with respect to the center of the dipole:

$$\frac{\partial\Gamma(\xi,\vec{r},\vec{b})}{\partial\xi} = \mathscr{K}\otimes\Gamma(\xi,\vec{r},\vec{b}) = \frac{3}{8\pi^3}\int d^2\rho_1\mu_G^2\left|g_S(R_1)K_1(\mu_G\rho_1)\frac{\vec{\rho}_1}{\rho_1} - g_S(R_2)K_1(\mu_G\rho_2)\frac{\vec{\rho}_2}{\rho_2}\right|^2 \times$$
$$\times\left[\Gamma\left(\xi,\vec{\rho}_1,\vec{b}+\frac{1}{2}\vec{\rho}_2\right)+\Gamma\left(\xi,\vec{\rho}_2,\vec{b}+\frac{1}{2}\vec{\rho}_1\right)-\Gamma(\xi,\vec{r},\vec{b})\right]. \qquad (32)$$

The calculation of the impact parameter integral (25) reduces Eq. (32) to Eq. (29). The calculation of the moment (27) leads to the integral equation for $\lambda(\xi,r)$. It is convenient to separate from the diffraction slope $B(\xi,r)$ the purely geometrical term $r^2/8$ related to the elastic form factor of the color dipole of the dipole moment r and to discuss instead of $\lambda(\xi,r)$ the function

$$\eta(\xi,r) = \lambda(\xi,r) - \frac{1}{8}r^2\sigma(\xi,r),$$

which satisfies the inhomogeneous integral equation

$$\frac{\partial\eta(\xi,r)}{\partial\xi} = \frac{3}{8\pi^3}\int d^2\rho_1\ \mu_G^2\left|g_S(R_1)K_1(\mu_G\rho_1)\frac{\vec{\rho}_1}{\rho_1} - g_S(R_2)K_1(\mu_G\rho_2)\frac{\vec{\rho}_2}{\rho_2}\right|^2 \times$$
$$\times\left\{\eta(\xi,\rho_1)+\eta(\xi,\rho_2)-\eta(\xi,r)+\frac{1}{8}(\rho_1^2+\rho_2^2-r^2)\left[\sigma(\xi,\rho_2)+\sigma(\xi,\rho_1)\right]\right\} =$$
$$= \mathscr{K}\otimes\eta(\xi,r)+\beta(\xi,r), \qquad (33)$$

where the inhomogeneous term equals

$$\beta(\xi,r) = \mathscr{L}\otimes\sigma(\xi,r) = \frac{3}{64\pi^3}\int d^2\rho_1\ \mu_G^2\left|g_S(R_1)K_1(\mu_G\rho_1)\frac{\vec{\rho}_1}{\rho_1} - g_S(R_2)K_1(\mu_G\rho_2)\frac{\vec{\rho}_2}{\rho_2}\right|^2 \times$$
$$\times(\rho_1^2+\rho_2^2-r^2)\left[\sigma(\xi,\rho_2)+\sigma(\xi,\rho_1)\right]. \qquad (34)$$

Because the homogeneous part of Eq. (33) coincides with the gBFKL equation (29), asymptotically the dipole cross section $\sigma(\xi,r)$ and the solution $\eta(\xi,r)$ of homogeneous Eq. (33) have identical energy dependence. Consequently, the solutions of homogeneous Eq. (33) give the asymptotically constant contribution to the diffraction cone and if $\sigma_a(\xi,r)$ is a solution of Eq. (29) and $\eta_a(\xi,r)$ is a solution of Eq. (33) with the diffraction slope $B_a(\xi,r)$, then $\eta_b(\xi,r) = \eta_a(\xi,r) + \Delta b\cdot\sigma_a(\xi,r)$, where $\Delta b = \text{const}$, is also a solution of Eq. (33) with the diffraction slope $B_b(\xi,r) = B_a(\xi,r) + \Delta b$. It is the inhomogeneous term, $\beta(\xi,r)$, which gives rise to $\eta(\xi,r)\propto\xi\sigma(\xi,r)$, i.e., to the asymptotic Regge growth of the diffraction slope, $B(\xi,r) = B(\xi_0,r) + 2\alpha'_{\mathbf{P}}\xi$, and the Regge term $2\alpha'_{\mathbf{P}}\xi$ does not depend on the size r of the dipole. Parametrically, $\alpha'_{\mathbf{P}}\propto\alpha_S(R_c)R_c^2$ times a small numerical factor. With the above specified infrared parameters $\alpha'_{\mathbf{P}}\approx 0.072\ \text{GeV}^{-2}$ was found in [28], for slopes of subleading trajectories see [29].

4. THE BEAM, TARGET AND EXCHANGE DECOMPOSITION OF THE DIFFRACTION SLOPE

To have more insight into the dipole-size dependence of the diffraction slope, it is useful to look at the scattering amplitude $\sigma(\xi,r,\vec{q})$ in terms of the gluon density matrix. For our

purposes, it is sufficient to treat the color structure of the proton in terms of the three valence (constituent) quarks. Then, as illustrated graphically in Fig. 1*b*, the unintegrated density matrix of gluons can be written as

$$\mathscr{F}\left(x,\vec{k}+\frac{1}{2}\vec{q},-\vec{k}+\frac{1}{2}\vec{q}\right)=\frac{4}{\pi}\int d^2k_1\mathscr{T}\left(\xi,\vec{k}+\frac{1}{2}\vec{q},-\vec{k}+\frac{1}{2}\vec{q},\vec{k}_1+\frac{1}{2}\vec{q},-\vec{k}_1+\frac{1}{2}\vec{q}\right)\times$$
$$\times\,\alpha_S(k_1^2)\left[G_1(q^2)-G_2\left(\vec{k}_1+\frac{1}{2}\vec{q},-\vec{k}_1+\frac{1}{2}\vec{q}\right)\right], \tag{35}$$

where $G_1(q^2)$ and $G_2(\vec{\kappa}_1,\vec{\kappa}_2)$ are the single- and two-quark form factors of the proton probed by gluons and $\mathscr{T}(\xi,\vec{k}+\vec{q},-\vec{k}+\vec{q}/2,\vec{k}_1+\vec{q},-\vec{k}_1+\vec{q}/2)$ stands for the propagation function of two t-channel gluons. In the Born approximation,

$$\mathscr{T}\left(\xi,\vec{k}+\frac{1}{2}\vec{q},-\vec{k}+\frac{1}{2}\vec{q},\vec{k}_1+\frac{1}{2}\vec{q},-\vec{k}_1+\frac{1}{2}\vec{q}\right)=\frac{\delta(\vec{k}-\vec{k}_1)}{\left[(\vec{k}+\vec{q}/2)^2+\mu_G^2\right]\left[(\vec{k}-\vec{q}/2)^2+\mu_G^2\right]}. \tag{36}$$

Splitting the color dipole vertex function into two pieces,

$$V_d(q,r)=\left[J_0\left(\frac{1}{2}qr\right)-J_0(kr)\right]=\left[J_0\left(\frac{1}{2}qr\right)-1\right]+\left[1-J_0(kr)\right],$$

we obtain a useful decomposition

$$\sigma(\xi,r,\vec{q})=\frac{4\pi}{3}\left[J_0\left(\frac{1}{2}qr\right)-1\right]\int\frac{d^2k}{k^4}\,\alpha_S(\kappa^2)\mathscr{F}\left(x,\vec{k}+\frac{1}{2}\vec{q},-\vec{k}+\frac{1}{2}\vec{q}\right)+$$
$$+\frac{4\pi}{3}\int\frac{d^2k}{k^4}\,\alpha_S(\kappa^2)\left[J_0(kr)-1\right]\mathscr{F}\left(x,\vec{k}+\frac{1}{2}\vec{q},-\vec{k}+\frac{1}{2}\vec{q}\right). \tag{37}$$

Because of the property defined by Eq. (14), the second term has the typical logarithmic k^2 integration. It comprises the contributions to the q dependence from the target and exchanged gluons. In contrast, such a logarithmic k^2 integration is absent in the first term; here the k^2 integration converges at finite $k^2\sim R_c^{-2}$.

The emerging representation

$$\sigma(\xi,r,\vec{q})=\frac{4\pi}{3}\left[J_0\left(\frac{1}{2}qr\right)-1\right]\int\frac{d^2k}{k^4}\,\alpha_S(\kappa^2)\mathscr{F}\left(x,\vec{k}+\frac{1}{2}\vec{q},-\vec{k}+\frac{1}{2}\vec{q}\right)+$$
$$+\frac{16}{9}\int\frac{d^2k}{k^4}\,\alpha_S(\kappa^2)\left[1-J_0(kr)\right]\int d^2k_1\mathscr{T}\left(\xi,\vec{k}+\vec{q},-\vec{k}+\frac{1}{2}\vec{q},\vec{k}_1+\frac{1}{2}\vec{q},-\vec{k}_1+\frac{1}{2}\vec{q}\right)\times$$
$$\times\,\alpha_S(k_1^2)\left[G_1(q^2)-G_2\left(\vec{k}_1+\frac{1}{2}\vec{q},-\vec{k}_1+\frac{1}{2}\vec{q}\right)\right] \tag{38}$$

nicely illustrates how the three relevant size parameters in the problem give rise to the three major components of the diffraction slope. The q dependence coming from the proton vertex function $V_p(\vec{k}_1,\vec{q})=G_1(q^2)-G_2(\vec{k}_1+\vec{q}/2,-\vec{k}_1+\vec{q}/2)$ is controlled by the proton size. The q dependence coming from the color dipole vertex function $V_d=J_0(qr/2)-1$ is controlled by the color dipole size r. The q dependence coming from $\mathscr{T}(\xi,\vec{k}+\vec{q}/2,-\vec{k}+\vec{q}/2,\vec{k}_1+\vec{q}/2,-\vec{k}_1+\vec{q}/2)$ depends on the effective k^2,k_1^2 which contribute to the scattering

amplitude and on the gluon propagation radius R_c. The latter scale remains important even at large k because the properties of the running gBFKL pomeron are controlled by interactions at $r \sim R_c$. In the asymptotic BFKL regime, at small x, the $\vec{k}_1$ and $\vec{k}$ become azimuthally uncorrelated.

In order to proceed further, one needs a model for $G_1(q^2)$ and $G_2(\vec{\kappa}_1, \vec{\kappa}_2)$. The radius R_N of the proton probed by the gluon can be different from the charge radius R_{ch}, still R_{ch} serves as a useful scale. The two-quark form factor $G_2(\vec{k}+\vec{q}/2, -\vec{k}+\vec{q}/2)$ is a steep function of k^2 and a smoother function of q^2 [41]. For instance, for the oscillator wave function of the 3-quark proton one readily finds

$$G_2\left(\vec{k}+\frac{1}{2}\vec{q}, -\vec{k}+\frac{1}{2}\vec{q}\right) = G_1\left(\frac{1}{4}q^2\right) G_1(3k^2). \tag{39}$$

A straightforward differentiation gives a transparent decomposition of $d\sigma(\xi, r, \vec{q})/dq^2$ into the following four terms:

$$\left.\frac{d\sigma(\xi, r, \vec{q})}{dq^2}\right|_{q^2=0} = \sum_{i=1}^{4} \left.\frac{d\sigma^{(i)}(\xi, r, \vec{q})}{dq^2}\right|_{q^2=0} = -\frac{16}{3}\int \frac{d^2k}{k^4}\alpha_S(\kappa^2)\left\{\frac{1}{16}r^2\int d^2k_1 \times\right.$$

$$\times \mathscr{T}(\xi, \vec{k}, -\vec{k}, \vec{k}_1, -\vec{k}_1)\alpha_S(k_1^2)\left[1-G_2(\vec{k}_1, \vec{k}_1)\right] - [1-J_0(kr)]\int d^2k_1\alpha_S(k_1^2) \times$$

$$\times \left[1-G_2(\vec{k}_1, \vec{k}_1)\right] \left.\frac{\partial \mathscr{T}\left(\xi, \vec{k}+\vec{q}/2, -\vec{k}+\vec{q}/2, \vec{k}_1+\vec{q}/2, -\vec{k}_1+\vec{q}/2\right)}{\partial q^2}\right|_{q^2=0} +$$

$$+ \frac{1}{6}R_N^2[1-J_0(kr)]\int d^2k_1 \mathscr{T}(\xi, \vec{k}, -\vec{k}, \vec{k}_1, -\vec{k}_1)\alpha_S(k_1^2) -$$

$$\left. - \frac{1}{24}R_N^2[1-J_0(kr)]\int d^2k_1 \mathscr{T}(\xi, \vec{k}, -\vec{k}, \vec{k}_1, -\vec{k}_1)\alpha_S(k_1^2)G_2(\vec{k}_1, \vec{k}_1)\right\}. \tag{40}$$

The following properties of $\mathscr{T}\left(\xi, \vec{k}+\vec{q}/2, -\vec{k}+\vec{q}/2, \vec{k}_1+\vec{q}/2, -\vec{k}_1+\vec{q}/2\right)$ are important in (40): First, in the infrared regulated QCD it is nonsingular at $k^2 = 0$, cf. Eq. (36). Second (modulo to the logarithmic scaling violations), its large-k^2 asymptotic is similar to that of the Born term (36), $\mathscr{T}\left(\xi, \vec{k}+\vec{q}/2, -\vec{k}+\vec{q}/2, \vec{k}_1+\vec{q}/2, -\vec{k}_1+\vec{q}/2\right) \propto 1/k^{-4}$. Third, in the Born approximation (after the azimuthal averaging)

$$\left.\frac{\partial \mathscr{T}\left(\xi, \vec{k}+\vec{q}/2, -\vec{k}+\vec{q}/2, \vec{k}_1+\vec{q}/2, -\vec{k}_1+\vec{q}/2\right)}{\partial q^2}\right|_{q^2=0} =$$

$$= -\frac{R_c^2}{(1+R_c^2k^2)^2}\mathscr{T}\left(\xi, \vec{k}+\frac{1}{2}\vec{q}, -\vec{k}+\frac{1}{2}\vec{q}, \vec{k}_1+\frac{1}{2}\vec{q}, -\vec{k}_1+\frac{1}{2}\vec{q}\right). \tag{41}$$

Fourth, finding the asymptotic Regge growth of the diffraction slope in [28] implies that in the high-energy limit $\xi \to \infty$ and for all $\vec{k}$ and $\vec{k}_1$

$$\left.\frac{\partial \mathscr{T}\left(\xi, \vec{k}+\vec{q}/2, -\vec{k}+\vec{q}/2, \vec{k}_1+\vec{q}/2, -\vec{k}_1+\vec{q}/2\right)}{\partial q^2}\right|_{q^2=0} =$$

$$= -\left[\alpha'_{\mathbf{P}}(\xi - \xi_0) + O(R_c^2)\right] \mathscr{T}\left(\xi, \vec{k} + \frac{1}{2}\vec{q}, -\vec{k} + \frac{1}{2}\vec{q}, \vec{k}_1 + \frac{1}{2}\vec{q}, -\vec{k}_1 + \frac{1}{2}\vec{q}\right). \qquad (42)$$

Consider first the decomposition of the diffraction slope for large dipoles, $r \gtrsim R_c$. In this limit, the cross section (38) is dominated by the contribution from $k^2 \sim \mu_G^2 = R_c^{-2} \gg R_N^{-2}$, so that $J_0(kr), G_1(3k^2) \ll 1$ and can be neglected and (cf. Eq. (9))

$$\sigma(\xi, r) = \frac{4\pi}{3} \int d^2k\, \alpha_S^2(k^2) \mathscr{F}(\xi, \vec{k}, \vec{k}).$$

Then, the first term in the expansion (40) can be evaluated as

$$\left.\frac{d\sigma^{(1)}(\xi, r, \vec{q})}{dq^2}\right|_{q^2=0} = -\frac{1}{2}\Delta b_1 \sigma(\xi, r) = -\frac{1}{16} r^2 \sigma(\xi, r). \qquad (43)$$

Similarly,

$$\left.\frac{d\sigma^{(3)}(\xi, r, \vec{q})}{dq^2}\right|_{q^2=0} = -\frac{1}{2}\Delta b_3 \sigma(\xi, r) = -\frac{1}{6} R_N^2 \sigma(\xi, r). \qquad (44)$$

The integrand of the fourth term in (40) contains the steeply decreasing two-body form factor $G_2(\vec{k}, -\vec{k})$, which cuts off the integration at $k^2 \lesssim R_N^2$. Consequently, one must distinguish between cases $r \lesssim R_N$ and $r \gtrsim R_N$. A simple estimate, which interpolates between these limiting cases, is

$$\left.\frac{d\sigma^{(4)}(\xi, r, \vec{q})}{dq^2}\right|_{q^2=0} = -\frac{1}{2}\Delta b_4 \sigma(\xi, r) = -\frac{1}{24} R_c^2 \sigma(\xi, r) \frac{r^2}{r^2 + R_N^2}. \qquad (45)$$

Notice that $\Delta b_4 \ll \Delta b_3$. Finally, making use of (42), the second term in (40) can be estimated as

$$\left.\frac{d\sigma^{(2)}(\xi, r, \vec{q})}{dq^2}\right|_{q^2=0} = -\frac{1}{2}\Delta b_2 \sigma(\xi, r) = -\left[\alpha'_{\mathbf{P}}(\xi - \xi_0) + O(R_c^2)\right] \sigma(\xi, r). \qquad (46)$$

At low energy, in the Born approximation, Eq. (41) gives $\Delta b_2 = 2R_c^2$. The salient feature of the resulting diffraction slope

$$B(\xi, r) = \sum_i \Delta b_i = \frac{1}{8} r^2 + \frac{1}{3} R_N^2 + 2\alpha'_{\mathbf{P}}(\xi - \xi_0) + O(R_c^2), \qquad (47)$$

is a presence of the geometrical contributions $\Delta b_1 = r^2/8$ and $\Delta b_3 = R_N^2/3$.

For large dipoles, $r \gtrsim R_c$, one recovers a sort of additive quark model, in which the uncorrelated gluonic clouds build up around the beam and target quarks and antiquarks, and the terms $O(R_c^2)$ and $2\alpha'_{\mathbf{P}}(\xi - \xi_0)$ describe the familiar Regge growth of diffraction slope for the quark–quark scattering. The opposite limit of small dipoles, $r \ll R_c$, is somewhat more tricky. In the second and third term in (40), the k^2 integration is cut off by $1 - J_0(kr)$ and extends up to A_σ/r^2, precisely as in the dipole cross section (10). Consequently, their contributions to the derivative (40) are still given by Eqs. (46) and (44), respectively, so that the Regge term and the contribution from the target proton size to expansion (47) are retained. The contribution from the first term in (40), i.e., from the size of the color dipole, changes dramatically and

will no longer have the geometric form $r^2/8$. Indeed, as we discussed following Eq. (37), the k^2 integration in the first term in (40) converges at $k^2 \lesssim R_c^2$. Consequently, in this limit $\kappa^2 = C^2/r^2$ and one can factor out $\alpha_S(\kappa^2) = \alpha_S(r)$ from the integrand. This leads to an estimate

$$\left.\frac{d\sigma^{(1)}(\xi, r, \vec{q})}{dq^2}\right|_{q^2=0} \approx -\frac{r^2}{16}\frac{\alpha_S(r)}{\alpha_S(R_c)}\sigma(\xi, R_c) \approx -\frac{r^2}{16}\frac{\pi^2}{3}\alpha_S(r)R_c^2 G\left(\xi, \frac{A_\sigma}{R_c^2}\right) \tag{48}$$

and, after making use of (11), to

$$\Delta b_1 = \frac{R_c^2}{8}\frac{G(\xi, A_\sigma/R_c^2)}{G(\xi, A_\sigma/r^2)}. \tag{49}$$

Similar considerations give an estimate for the contribution to the diffraction slope from the fourth term in (40), which is a negligible correction to Δb_1:

$$\Delta b_4 = \frac{R_c^2}{12}\frac{R_c^2}{R_N^2}\frac{G(\xi, A_\sigma/R_c^2)}{G(\xi, A_\sigma/r^2)}. \tag{50}$$

More comments on Δb_1 are in order. At asymptotically large ξ and/or asymptotically small x, the running gBFKL approach predicts the universal x dependence of the gluon structure function [17]

$$G(x, Q^2) \propto \left[\frac{1}{\alpha_S(Q^2)}\right]^\gamma \left(\frac{1}{x}\right)^{\Delta_{\mathbf{P}}}, \tag{51}$$

where $\gamma = 12\Delta_{\mathbf{P}}/\beta_0$ and $\beta_0 = 11 - 2n_f/3$. Consequently, in the well developed BFKL regime Δb_1 will not depend on energy:

$$\Delta b_1 = \frac{R_c^2}{8}\left[\frac{\alpha_S(r)}{\alpha_S(R_c)}\right]^\gamma. \tag{52}$$

However, at moderately small x values, the x dependence of the gluon structure function exhibits strong dependence on the factorization scale, the ratio $G(\xi, A_\sigma/R_c^2)/G(\xi, A_\sigma/r^2)$ has a substantial x dependence and Δb_1 contributes to the energy dependence of the diffraction cone. Specifically, it makes the slope of the effective Regge trajectory α'_{eff} substantially larger than the true slope of the leading Pomeron trajectory $\alpha'_{\mathbf{P}}$ [28].

To summarize, the geometrical contribution to the diffraction slope from the target proton size, $\Delta b_3 = (1/3)R_N^2$, persists for all the dipole sizes (the term Δb_4 which is also associated with the proton size is negligibly small in all cases). Although the nonperturbative parameter R_N^2 is not calculable from first principles, its contribution to the diffraction slope varies neither with energy nor with the dipole size and can eventually be fixed from the accurate experimental data.

5. SOFT POMERON AND DIFFRACTIVE SCATTERING OF LARGE COLOR DIPOLES

The need for a soft pomeron contribution in addition to the gBFKL dipole cross section described previously is brought about by phenomenological considerations. A viable gBFKL

phenomenology of the rising component of the proton structure function over the whole range of Q^2 studied at HERA (real photoabsorption included) is obtained if one starts with the Born dipole cross section $\sigma_B(r)$ as a boundary condition for the gBFKL evolution at $x_0 = 0.03$ [26, 27]. However, such a $\sigma_B(r)$ falls short of the interaction strength at $r \gtrsim R_c$; roughly speaking, for the phenomenological value $R_c = 0.27$ fm one finds $\sigma_B(r \gtrsim 1 \text{ fm}) \sim 5$ mb, whereas for the description of soft processes one rather needs the dipole cross section ~ 50 mb at $r \gtrsim 2$ fm. Therefore, at $r \gtrsim R_c$, the above described perturbative gBFKL dipole cross section (which hereafter we supply with the subscript «pt») $\sigma_{pt}(\xi, r)$, must be complemented by the contribution from the nonperturbative soft pomeron, $\sigma_{npt}(\xi, r)$. Because in all the cases studied the contribution from $\sigma_{pt}(\xi, r)$ exhausts the rise of the total cross sections and/or of the proton structure function, in Refs. 26 and 5 we have modeled the soft nonperturbative pomeron by the energy independent $\sigma_{npt}(\xi, r) = \sigma_{npt}(r)$. For the lack of better theoretical and experimental information as well as simplicity, we make the simplest possible assumption that the eikonals for the perturbative and soft interactions are additive, which to the lowest order amounts to additivity of the dipole cross sections $\sigma(\xi, r) = \sigma_{pt}(\xi, r) + \sigma_{npt}(r)$.

The direct determination of the total dipole cross section $\sigma(\xi, r)$ from the experimental data on photo- and leptoproduction of vector mesons is reported in [9] and supports the flavor independence of $\sigma(\xi, r)$. Other constraints for $\sigma_{npt}(r)$ include real photoproduction [5, 10], hadronic diffractive scattering [24], nuclear shadowing in deep inelastic scattering [42], diffractive deep inelastic scattering at HERA [43, 44], nuclear attenuation in photoproduction of light vector mesons and the onset of color transparency in leptoproduction of vector mesons [4] and the proton structure function at moderate and small Q^2 [26, 27]. All the results are consistent with the form of the dipole cross section suggested in [24, 26, 5], a convenient parameterization for which is

$$\sigma_{npt}(r) = \sigma_0 \left[1 - \sum_{i=1}^{2} A_i \exp\left(-\frac{r^2}{a_i^2}\right)\right] \left[1 + \sum_{i=1} D_i \exp\left(-\frac{(r-b_i)^2}{c_i^2}\right)\right] \tag{53}$$

with $\sigma_0 = 41.2$ mb, $A_1 = 1.45$, $A_2 = -0.45$, $a_1 = 1.30$ fm, $a_2 = 0.75$ fm, $D_1 = 0.80$, $D_2 = 0.36$, $b_1 = 0.88$ fm, $b_2 = 2.08$ fm, $c_1 = 0.53$ fm, and $c_2 = 1.14$ fm. For a somewhat cruder fit with $D_i = 0$ we find $\sigma_0 = 51.6$ mb, $A_1 = 1.82$, $A_2 = -0.82$, $a_1 = 1.05$ fm, and $a_2 = 0.72$ fm. For small dipoles, $r \ll R_c$, this cross section is poorly known because it is swamped by $\sigma_{pt}(\xi, r)$.

There is nothing unusual in the concept of a nonperturbative cross section. The conventional gluon structure function of the photon,

$$G(x, Q^2) = \int_0^{Q^2} \frac{dk^2}{k^2} \mathcal{F}(x, \vec{k}, -\vec{k}),$$

always contains a contribution from gluons with soft transverse momenta $k^2 < Q_0^2 \lesssim 1$ GeV^2, which persists at all Q^2 and equals precisely $G(x, Q_0^2)$, the familiar input to the conventional GLDAP analysis of the Q^2 evolution of parton densities. One is perfectly content with the strong sensitivity of the GLDAP evolution to this unknown soft input $G(x, Q_0^2)$, which is routinely fixed from fits to the experimental data. In the color dipole approach to DIS, our soft dipole cross section $\sigma_{npt}(r)$ plays exactly the same role as the gluon (quark) structure functions at a soft scale Q_0^2. Furthermore, it is tempting to reinterpret this soft dipole cross section $\sigma_{npt}(r)$ in terms of the nonperturbative gluon distribution in the spirit of Eq. (10). The models of

soft scattering via polarization of the nonperturbative QCD vacuum [36, 11] belong to this category and give $\sigma_{npt}(r)$ very similar to our parameterization (53). In the interesting region of $r \lesssim 1$–1.5 fm, the conservative estimate of uncertainties in $\sigma_{npt}(r)$ is 10-20%, the major source of uncertainty being due to absorption corrections. For heavy quarkonia the absorption correction are negligible [5].

We shall assume the conventional Regge rise of the diffraction slope for the soft pomeron,

$$B_{npt}(\xi, r) = \Delta B_d(r) + \Delta B_N + 2\alpha'_{npt}(\xi - \xi_0)\,,$$

where $\Delta B_d(r)$ and ΔB_N stand for the contribution from the beam dipole and target nucleon size and $\xi_0 = \log(1/x_0)$. As a guidance we take the experimental data on the pion–nucleon scattering [45], which suggest $\alpha'_{npt} = 0.15$ GeV^{-2} (for the small α'_{npt} descriptions of nucleon–nucleon scattering see [46]). A plausible guess for the proton size contribution is

$$\Delta B_N = \Delta b_3 = \frac{1}{3} R_N^2\,. \tag{54}$$

In the energy independent soft exchange for small dipoles, $\Delta B_d(r)$ is likely to follow the geometric law $\Delta B_d(r) \approx r^2/8$ as in Eq. (43). Extension of this law to large dipoles is questionable. The large-r saturation of $\sigma_{npt}(r)$ as parameterized by (53) is a simplifying assumption; what happens at $r \gg 1$ fm is immaterial because even in hadrons the probability of finding large dipoles, $r \gg 1$ fm, is negligible. However, the diffraction slope is more sensitive to the large dipole contribution. For instance, if scattering of large dipoles of size $r \gtrsim R_N$ is modeled by scattering of thin classical strings off the strongly absorbing target nucleon of radius R_N, then for large dipoles (strings), $r \gtrsim 2R_N$, one readily finds the profile function

$$\Gamma(b, r) \approx \theta(R - b) + \frac{2}{\pi}\theta(b - R)\theta\left(R + \frac{1}{2}r - b\right) \arcsin\frac{R}{b}\,,$$

which gives the large-r behavior, $\sigma_{npt}(r) \approx 2R_N r$, and the tamed rise of the diffraction slope $\Delta B_d(r \gg 1\,\text{fm}) \sim r^2/24$. This consideration suggests the interpolation formula of the form

$$B_d(r) = \frac{r^2}{8}\,\frac{r^2 + aR_N^2}{3r^2 + aR_N^2}\,, \tag{55}$$

where a is a phenomenological parameter, $a \sim 1$.

Such a taming of the growth of $B_d(r)$ is supported by the phenomenology of πN scattering. Let us take for pion the oscillator wave function and assume that the gluon probed radius of the pion equals the charge radius. Then, the contribution from the pion size to the diffraction slope for the purely geometrical form (43) for $B_d(r)$ gives the unacceptably large value

$$\Delta B_\pi = \frac{1}{8}\,\frac{\langle\pi|r^2[\sigma_{pt}(x_0, r) + \sigma_{npt}(r)]|\pi\rangle}{\langle\pi|[\sigma_{pt}(x_0, r) + \sigma_{npt}(r)]|\pi\rangle} \approx 9.7\ \text{GeV}^{-2}\,.$$

Taking for the contribution from the proton size ΔB_N the estimate (54) we end up with $B_{\pi N} \approx$ ≈ 15 GeV^{-2}, which substantially exceeds the experimental result $B_{\pi N}(\nu = 200\ \text{GeV}) =$ $= 9.9 \pm 0.1$ GeV^{-2} [45]. The discrepancy increases further if one adds to the above theoretical estimate the Regge term $2\alpha'_{npt}(\xi - \xi_0) \approx 1$ GeV^{-2} evaluated using the relationship between the x_{eff} and pion energy, $x_{eff} \approx m_V^2/2\nu m_p$.

What is the origin of this discrepancy? If $\sigma(\xi, r)$ was r independent and if the gluon probed and charge radii of the pion were identical, then one would find from (5) the familiar

$$\Delta B_\pi(\xi_0) = \frac{1}{3}\langle R^2_{ch}\rangle_\pi \approx 4 \text{ GeV}^{-2}. \tag{56}$$

With our parameterization (53), the soft dipole cross section keeps rising at $r \sim 1$ fm and for this reason the matrix element (5) is dominated by r^2 larger than in the charge radius of the pion, and we end up with ΔB_π larger than an expectation (56) based on the charge radius of the pion. The matrix element (5) can be made smaller and compatible with the experiment at the expense a rapid saturation of the soft cross section for large dipoles, $\sigma_{npt}(r \gtrsim 1 \text{ fm}) \approx \sigma_{tot}(\pi N)$, when one shall recover the estimate (56). This solution must be rejected, because it would lead to negligible fluctuations of the soft dipole cross section in conflict with the experimental data on the diffraction dissociation of pions, which require

$$\frac{\langle\pi|\sigma^2(\nu_0, r)|\pi\rangle - \langle\pi|\sigma(\nu_0, r)|\pi\rangle^2}{\langle\pi|\sigma(\nu_0, r)|\pi\rangle^2} \approx 0.5. \tag{57}$$

An attempt to retain the geometrical law and still agree with the experiment at the expense of taking $\Delta B_N \sim 0$ must be rejected too. We believe that the string model suggested taming of $B_d(r)$ Eq. (55) is a more acceptable solution. Hereafter we take $\Delta B_N = \Delta b_3 = 4.8$ GeV^{-2}. Then the pion–nucleon diffraction slope is reproduced with reasonable values of the parameter a in the formula (55): $a = 1.2$ for $\alpha'_{npt} = 0.1$ GeV^{-2} and $a = 0.9$ for $\alpha'_{npt} = 0.15$ GeV^{-2}. Hereafter we shall use the latter set of parameters.

6. SOFT-HARD DECOMPOSITION OF TOTAL CROSS SECTIONS FOR VN SCATTERING

We start presentation of our results from an evaluation of the vector meson-nucleon total cross section

$$\sigma_{tot}(VN) = \frac{N_c}{2\pi}\int_0^1 \frac{dz}{z^2(1-z)^2}\int d^2r\left\{m_q^2\phi(r,z)^2 + \left[z^2+(1-z)^2\right]\left[\partial_r\phi(r,z)\right]^2\right\}\sigma(x_{eff}, r). \tag{58}$$

For the parameterization of lightcone wave functions $\phi(r, z)$ of vector mesons see [10]. The results for $x_{eff} \leq x_0 = 0.03$ are shown in Fig. 2 (left box). The smaller is the radius of the vector meson V the smaller is the total cross section $\sigma_{tot}(VN)$, to a crude approximation, $\sigma_{tot}(VN) \propto R_V^2$, excepting the radial excitations ϕ', ρ'.

In Fig. 2 (left box) we show separately the soft pomeron contribution to $\sigma_{tot}(VN)$. For the J/Ψ the radius is large, $R_{J/\Psi} \approx 0.4$ fm $> R_c = 0.27$ fm and the soft contribution is substantial; for the Υ the soft contribution is a small correction to the dominant perturbative contribution. At subasymptotic energies, the gBFKL approach predicts steeper rise with energy for smaller dipoles, cf. Eq. (11), the trend which is clearly seen in Fig. 2 (left box). At asymptotic energies the contribution from the rising gBFKL cross section takes over for all channels. In [47] it has been observed that for the «magic» radius $r_\Delta \sim 0.15$ fm $\sim R_c/2$ the gBFKL color dipole cross section exhibits the precocious asymptotic energy dependence $\sigma_{pt}(x, r_\Delta) \propto x^{-\Delta_{\mathbb{P}}}$. Because $R_\Upsilon \approx 0.18$ fm is very close to the «magic» radius r_Δ, the predicted energy dependence of the perturbative contribution to $\sigma_{tot}(\Upsilon N)$ is very close to $\propto W^{2\Delta_{\mathbb{P}}} = W^{0.8}$.

The case of the Ψ' is interesting for its large radius $R_{\Psi'} \approx 0.8$ fm and large soft contribution. Because the Ψ' and ϕ^0 have very close radii, the useful comparison is with $\sigma_{tot}(\phi N)$. For small W, $\sigma_{tot}(\Psi' N)$ of the present paper is indeed numerically very close to $\sigma_{tot}(\phi^0 N)$ calculated in [10], but the rise of $\sigma_{tot}(\Psi' N)$ by $\sim 50\%$ from $W \sim 10$ GeV to $W \sim 500$ GeV is much weaker than the rise of $\sigma_{tot}(\phi N)$ by almost a factor 2 over the same energy range. With our energy independent $\sigma_{npt}(r)$, the rise of $\sigma_{tot}(\Psi' N)$ is entirely due to the perturbative gBFKL cross section $\sigma_{pt}(\xi, r)$, which rises with energy more steeply at small r. Although the Ψ' and the ϕ^0 have similar mean square radii, because of the node effect the relative contribution of small r for the case of $\Psi' N$ is smaller than for the case of ϕN and this explains the counterintuitive difference of the energy dependence of the two cross sections.

7. DIFFRACTIVE PRODUCTION CROSS SECTIONS FOR THE 1S STATES J/Ψ AND Υ

Now we turn to the vector meson production. The strong point about color dipole factorization equations (13), (14), (19), and (20) is that apart from the trivial factors C_V and C_V/m_V the production amplitudes are flavor independent when considered as a function of the scanning radius r_S and/or $Q^2 + m_V^2$ [3–5, 28, 10]. To this end, Eqs. (13), (14), (19), and (20) represent the leading twist terms and the correct twist expansion goes in powers of $1/(Q^2+m_V^2)$ rather than in powers of $1/Q^2$. For instance, in [10] we have shown how the ratio of the J/Ψ and ρ production cross sections becomes remarkably constant when the two cross sections are taken at equal $Q^2 + m_V^2$ in contrast to a variation by about three orders in magnitude when the two cross sections are compared at equal Q^2. For this reason we strongly advocate the presentation of the experimental data as a function of the flavor-symmetry restoring variable $Q^2+m_V^2$ rather than Q^2 and whenever appropriate we present our results in terms of this scaling variable.

The soft/hard decomposition of production amplitudes depends on the relationship between

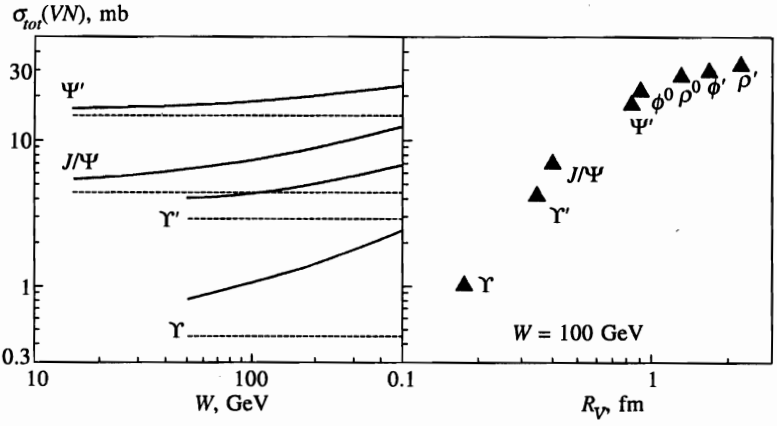

Fig. 2. The left box corresponds to the color dipole model predictions for the total cross section $\sigma_{tot}(VN)$ for the interaction of the heavy vector mesons J/Ψ, Ψ', Υ, and Υ' with the nucleon target as a function of c.m.s. energy W. The dashed curve represents the soft pomeron contribution. The right box shows the color dipole model predictions for the total cross section $\sigma_{tot}(VN)$ vs. radius R_V of vector mesons ρ^0, ρ', ϕ^0, ϕ', J/Ψ, Ψ', Υ, and Υ'

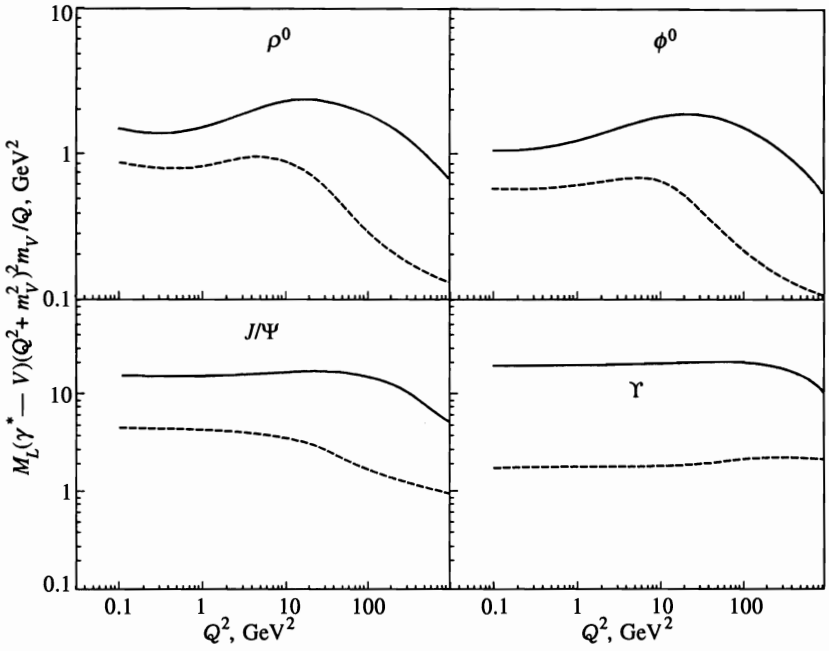

Fig. 3. Decomposition of production amplitude for longitudinally polarized vector mesons into soft (dashed curves) and perturbative+soft (solid curves) contribution as a function of $Q^2 + m_V^2$. The nonmonotonic Q^2 dependence is due to the increase of x_{eff} at fixed $W = 150$ GeV

r_S and R_c. The hard contribution dominates at $r_S \lesssim R_c$, i.e., if

$$Q^2 + m_V^2 \gtrsim \frac{A^2}{Rc^2} \sim 30 \text{ GeV}^2, \tag{59}$$

which holds better for the heavier vector mesons and the larger Q^2. Our phenomenological soft interaction, as well as other models for the soft pomeron [36, 11], extends well into $r \lesssim R_c$. Arguably, with better understanding of the perturbative gBFKL amplitude, one can eventually use the vector meson production for better fixing the effect of soft interactions at short distances. In Fig. 3 we show our decomposition of the production amplitudes into the hard (perturbative) and soft contribution as a function of Q^2 for different vector mesons at the typical HERA energy $W = 150$ GeV. Because for the lighter mesons the pQCD scale parameter is smaller, $\tau_L(\rho^0) < \tau_L(J/\Psi) < \tau_L(\Upsilon)$, the soft contribution is somewhat larger for the lighter quarkonia.

Regarding a comparison with the experimental data, the most straightforward theoretical predictions are for the forward production, and we calculate $(d\sigma/dt)_{t=0}$ and $B(t = 0)$. The experimental determination of these quantities requires extrapolations of $d\sigma/dt$ to $t = 0$, which is not always possible and one often reports the t-integrated production cross sections. The principal lesson from the high precision $\pi^{\pm}N$ scattering experiments is that the diffraction slope $B(t)$ depends strongly on the region of t and for average $\langle t \rangle \sim 0.1$–$0.2$ GeV^2 which dominate the integrated total cross section, the diffraction slope is smaller than at $t = 0$ by ~ 1 GeV^{-2} [45]. We take these πN scattering data for the guidance, and for more direct comparison with the presently available experimental data instead of the directly calculated $B(t = 0)$ in all the cases we report

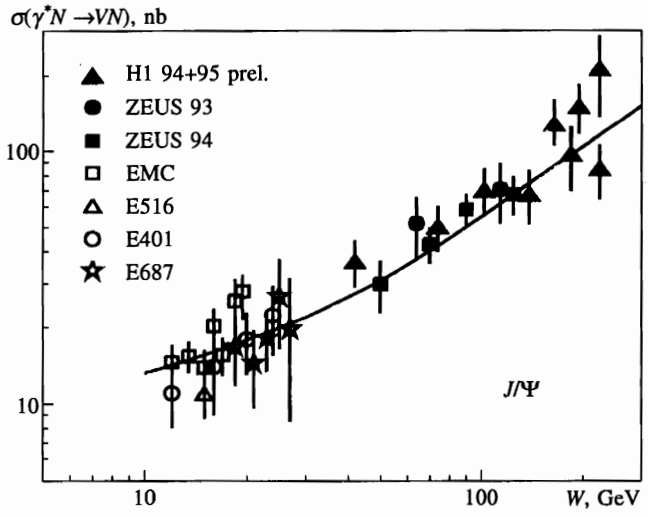

Fig. 4. The color dipole model predictions for the W dependence of the real photoproduction cross section $\sigma(\gamma^* \to V)$ for the J/Ψ production vs. the low-energy EMC [48], E516 [49], E401 [50], E687 [51] and high-energy ZEUS [52, 53] and H1 [54–56] data

$$B = B(t=0) - 1 \text{ GeV}^{-2} \tag{60}$$

which we also use for the evaluation of the t-integrated production cross section from the theoretically calculated $(d\sigma/dt)_{t=0}$:

$$\sigma(\gamma^* \to V) = \frac{1}{B} \left.\frac{d\sigma(\gamma^* \to V)}{dt}\right|_{t=0}. \tag{61}$$

The uncertainties in the value of B and with the evaluation (61) presumably do not exceed 10% and can be reduced when more accurate data will become available.

We start presentation of our results and comparison with the available experimental data with real photoproduction of the J/Ψ in Fig. 4. The agreement with experimental data from the fixed target experiments (EMC [48]; E516 [49]; E401 [50]; E687 [51]) and from the HERA experiments (ZEUS [52, 53]; H1 [54–56]) is good in the both magnitude and energy dependence of the cross section. For the J/Ψ and $Q^2 = 0$ the scanning radius is still large, $r_s \approx 0.4$ fm, and at smaller energies $W \simeq 15$ GeV the soft contribution makes $\sim 50\%$ of the photoproduction amplitude. Still, it is smaller than in $\sigma_{tot}(J/\Psi N)$ and $\sigma(\gamma \to J/\Psi)$ rises much faster that $\sigma^2_{tot}(J/\Psi N)$, which is one of examples of the failure of the vector dominance model for processes with heavy quarkonia. Recall that VDM predicts $\sigma(\gamma \to J/\Psi) \propto \sigma^2_{tot}(J/\Psi N)$.

The relationship (14) (and also (7)) is to a large extent the model independent one and predicts the dominance of σ_L at large Q^2. It is convenient to present the results for $R = \sigma_L/\sigma_T$ in the form of the ratio

$$R_{LT} = \frac{m_V^2}{Q^2} \left.\frac{d\sigma_L(\gamma^* \to V)}{d\sigma_T(\gamma^* \to V)}\right|_{t=0} \tag{62}$$

shown in Fig. 5 (m_V is the mass of the vector meson). The point made in [4, 5] and in a somewhat different form repeated in [6] is that compared to $\mathcal{M}_L$ the transverse amplitude $\mathcal{M}_T$

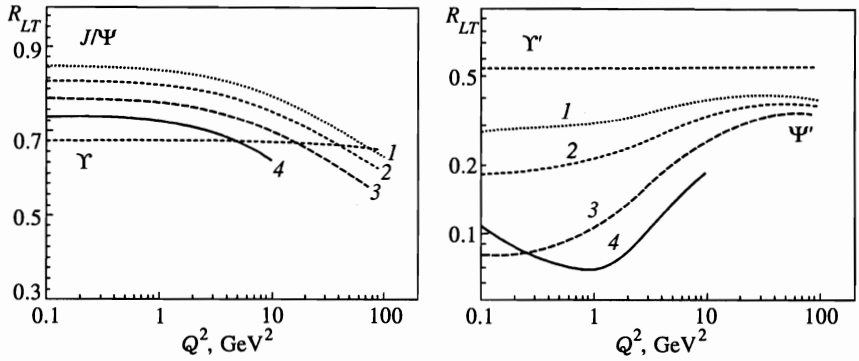

Fig. 5. The color dipole model predictions for the Q^2 and W dependence of the ratio of the longitudinal and transverse differential cross sections in the form of the quantity given by Eq. (62) for W = 500 GeV (curve *1*), 150 GeV (curve *2*), 50 GeV (curve *3*), and 15 GeV (curve *4*)

receives larger contribution from large r asymmetric end-point configurations with $z(1-z) \ll 1$. For this reason $R_{LT} < 1$ and is steadily decreasing with Q^2. The steeper rise of $\sigma_{pt}(x,r)$ at smaller r makes the end-point contributions less important at higher energies and R_{LT} rises with energy, although very weakly. The above predictions for $R = d\sigma_L/d\sigma_T$ must be tested at $t = 0$, the present experimental data on R are for the t-integrated cross sections. In [8] it has been argued that at large t rather $\sigma_T \gg \sigma_L$, so that the ratio R measured experimentally for the t integrated cross sections can be somewhat smaller than our predictions for $t = 0$. The calculation of the t-dependence of R_{LT} is an interesting subject on its own and goes beyond the scope of the present analysis.

In the typical HERA kinematics the longitudinal polarization parameter $\epsilon \approx 1$ and as our predictions for polarization unseparated production cross section we present

$$\sigma(\gamma^* \to V) = \sigma_T(\gamma^* \to V) + \sigma_L(\gamma^* \to V).$$

In Fig. 6 we show our predictions for the J/Ψ and Υ production. The short hand representation of the same results is in terms of the exponent of the energy dependence of the t-integrated $\sigma(\gamma^* \to V) \propto W^\delta = W^{4\Delta_{eff}}$ and/or $d\sigma/dt|_{t=0} \propto W^\delta = W^{4\Delta_{eff}}$. The exponent δ for the t-integrated cross section is slightly smaller because of the shrinkage of the diffraction cone. The effective intercept Δ_{eff} depends on the range of W the fit is made (the more detailed discussion of this issue is found in [5]), in Fig. 7 we present our evaluations for W = 100 GeV. For the sake of completeness, we show on the same plot Δ_{eff} for light vector mesons evaluated from cross sections calculated in Ref. 10. Slight departures from exact flavor symmetry are due to slight differences in the pQCD scale factors $\tau(V)$ for different vector mesons. The predicted downwards turn of Δ_{eff} at very large Q^2 is due to the increase of x_{eff} at fixed W. The real photoproduction of Υ offers one of the best determinations of the intercept $\Delta_{\mathbf{P}}$ of the gBFKL pomeron, because in this case one has the magic scanning radius $r_S \sim R_c/2$ and we indeed find $\Delta_{eff} \approx \Delta_{\mathbf{P}} = 0.4$. The usual fits to the experimental data are of the form $\sigma(\gamma^* p \to Vp) \propto W^\delta = W^{4\Delta_{eff}}$. The evaluated value of $\delta \simeq 0.9$ from Fig. 4 in the range $40 < W < 140$ GeV is in good agreement with the value $\delta = 0.92 \pm 0.14(\text{stat.}) \pm 0.10(\text{syst.})$ extracted from the data on elastic J/Ψ photoproduction [53]. Analogous estimation of $\delta \sim 0.82$ from Fig. 4 in the range $30 < W < 240$ GeV is in good agreement with the value $\delta = 0.77 \pm 0.13$ presented in [56]. The recent H1 data on elastic virtual photoproduction of J/Ψ [56] reported

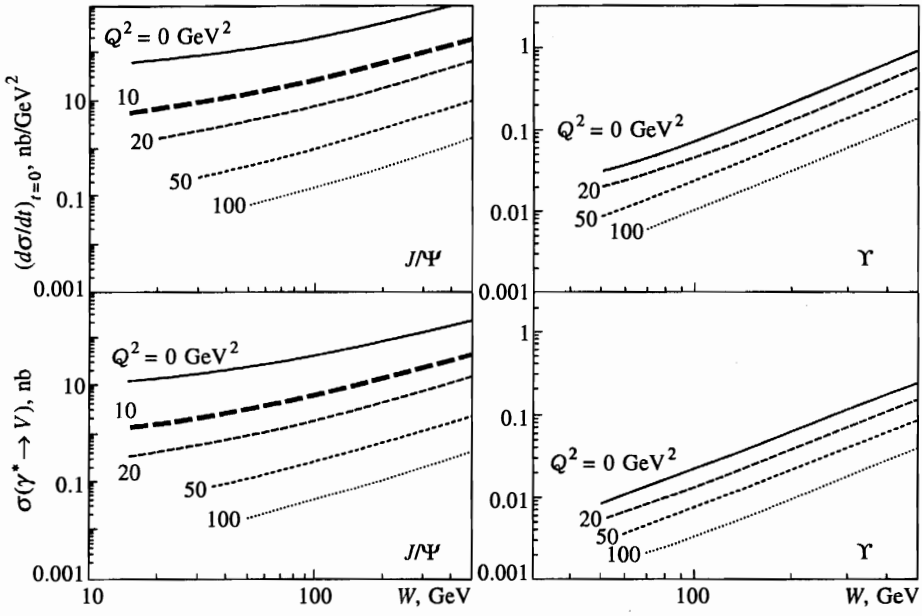

Fig. 6. The color dipole model predictions for the polarization-unseparated forward differential cross section (top boxes) $[d\sigma(\gamma^* \to V)/dt]_{t=0} = [d\sigma_T(\gamma^* \to V)/dt]_{t=0} + [d\sigma_L(\gamma^* \to V)/dt]_{t=0}$ for the J/Ψ and Υ production as a function of the c.m.s. energy W at different values of Q^2. The bottom boxes are predictions for the polarization-unseparated t-integrated cross section $\sigma(\gamma^* \to V) = \sigma_T(\gamma^* \to V) + \sigma_L(\gamma^* \to V)$

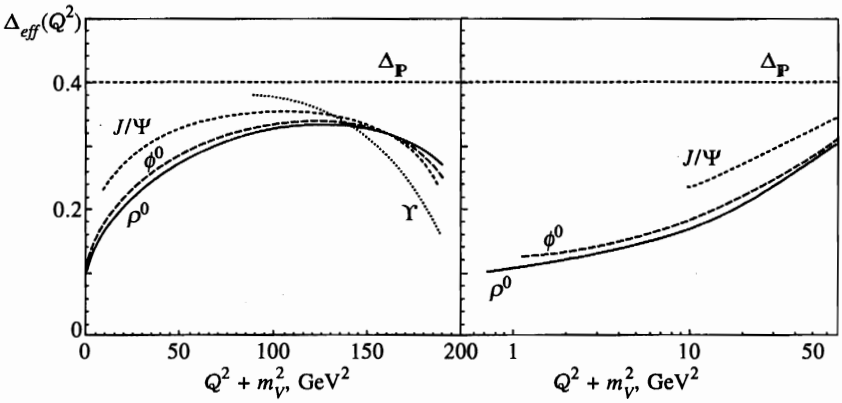

Fig. 7. The Q^2 dependence of the effective intercept $\Delta_{eff}(Q^2)$ for the forward production of ρ^0, ϕ^0, J/Ψ, and Υ at $W = 100$ GeV

the values of $\delta = 1.07 \pm 0.57$ at $Q^2 = 3.7$ GeV^2 and 1.22 ± 0.52 at $Q^2 = 16$ GeV^2 in the energy range $40 < W < 150$ GeV, which correspond with our results $\delta = 0.98$ and $\delta = 1.15$, respectively.

The salient features of the Q^2 dependence are best seen when cross sections are plotted as a function of the flavor symmetry restoring variable $Q^2 + m_V^2$, when the J/Ψ and Υ production

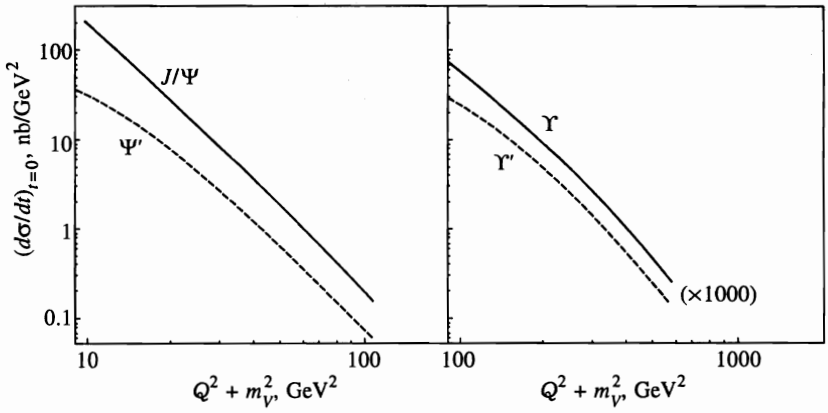

Fig. 8. The color dipole model predictions for the dependence on the scaling variable $Q^2 + m_V^2$ of the polarization-unseparated $[d\sigma(\gamma^* \to V)/dt]_{t=0} = [d\sigma_T(\gamma^* \to V)/dt]_{t=0} + [d\sigma_L(\gamma^* \to V)/dt]_{t=0}$ at the HERA energy $W = 100$ GeV

cross section exhibit very similar dependence (Fig. 8). With $R_{LT} \approx 1$ the theory predicts

$$\left.\frac{d\sigma}{dt}\right|_{t=0} \sim \frac{1}{(Q^2+m_V^2)^3} G^2\left(x_{eff}, \tau(V)(Q^2+m_V^2)\right). \tag{63}$$

If one fits (63) to the $(Q^2+m_V^2)^{-n}$ behavior and neglects the Q^2 dependence coming from the gluons structure function, then $n \approx 3$. The effect of the gluon structure function is twofold. At a fixed x_{eff}, i.e., when energy changes with Q^2 according to $W^2 = (Q^2+m_V^2)/x_{eff}$, the gluon structure function rises with Q^2, which lowers the fitted exponent n: $n \lesssim 3$. On the other hand, experimentally one usually studies the Q^2 dependence at fixed energy W, when $x_{eff} = (Q^2+m_V^2)/W^2$ increases with Q^2. Because the gluon structure decreases towards large x, this induced Q^2 dependence enhances the exponent n. The exponent n depends on the range of Q^2 the fit is performed in. For instance, in the J/Ψ production at a typical HERA energy $W = 100$ GeV we predict $n \approx 2.8$ for the semiperturbative region of $Q^2 \lesssim 10$ GeV^2 and $n \approx 3.2$ if the fit is performed in the region of $15 \lesssim Q^2 \lesssim 100$ GeV^2. We recall that for the ρ^0 production we found $n \approx 2.4$ $Q^2 \lesssim 10$ GeV^2 and $n \approx 3.2$ for $15 \lesssim Q^2 \lesssim 100$ GeV^2 [10]. The results for the Υ are similar to the large-Q^2 result for the J/Ψ. The departures from the exact flavor symmetry due to $R_{LT} \neq 1$ and slight flavor dependence of the pQCD scale $\tau(V)$ are marginal for all the practical purposes.

The experimental data on virtual photoproduction of charmonium states are still scanty and there are no data yet on the photoproduction of bottonium. In Fig. 9 we present a summary of the experimental data on the J/Ψ production from the fixed target EMC experiment [48] and the ZEUS [52, 57] and H1 [54, 56, 58] experiments at HERA. The theoretical results are for $W = 15$ GeV appropriate for the EMC experiment (the dashed curve) and for $W = 100$ GeV appropriate for the HERA experiments, there is a reasonable agreement between the theory and experiment. One of the outstanding experimental problems at large Q^2 is a separation of elastic reaction $\gamma^* p \to V + p$ from the inelastic background $\gamma^* p \to V + X$ and the low-energy EMC data are well known to have been plagued by the inelastic background. The contribution from inelastic background to the experimental cross section may be the reason why we underestimate the experimental data. One more argument on favor of this point will be presented in the discussion below of the diffraction slope.

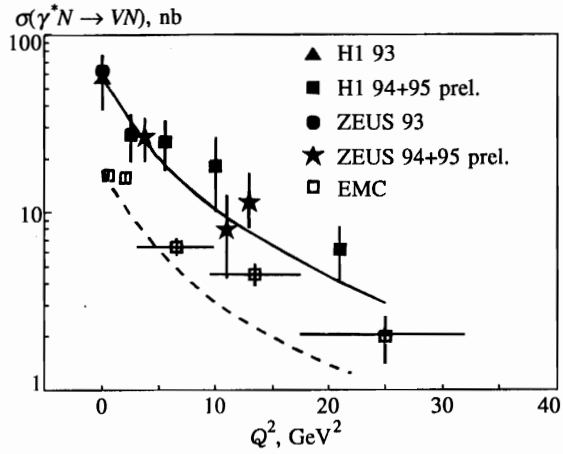

Fig. 9. The color dipole model predictions for the Q^2 dependence of the observed cross section $\sigma(\gamma^* \to V) = \sigma_T(\gamma^* \to V) + \epsilon\sigma_L(\gamma^* \to V)$ of exclusive J/Ψ production vs the low-energy (EMC [48]) and high-energy (ZEUS [52, 57], H1 [54, 56, 58]) data

8. DIFFRACTION CONE FOR THE $V(1S)$ STATES

Evidently, the contribution to the diffraction slope from the $\gamma^* \to V$ transition vertex decreases with the decreasing scanning radius r_S, i.e., with rising Q^2 [28]. At fixed energy W the value of x_{eff} rises and the rapidity ξ decreases which also diminishes the diffraction slope because the Regge term becomes smaller which is an important component of the Q^2 dependence at fixed W. In this section we report evaluations of the diffraction slope based on Eq. (28). We use the results of Ref. 28 for the energy and dipole size dependence of $B(\xi, r)$ for gBFKL color dipole amplitude. For the soft pomeron contribution, we use the parameterizations (53) and (55). According to Fig. 3, the nonperturbative contribution to the J/Ψ and Υ production amplitudes is small, and our results for the diffraction slope are insensitive to the soft pomeron effects. Our definition of the diffraction slope is Eq. (60) in Sec. 7 and is meant to correspond to the experimentally measured slope $B(t)$ at $t \simeq 0.1$–0.15 GeV^{-2}.

As it was shown in [28], at subasymptotic energies the diffraction slope for the gBFKL amplitude grows rather rapidly, by $\simeq 1.4$ GeV^{-2} when W grows by one order in magnitude from the fixed-target energy $W = 15$ GeV up to the HERA energy $W = 150$ GeV. This corresponds to the effective shrinkage rate $\alpha'_{eff} \approx 0.15$ GeV^{-2}, only at very high energy beyond the HERA range the shrinkage will follow the true slope of the Regge trajectory for the rightmost gBFKL singularity $\alpha'_{\mathbb{P}} = 0.07$ GeV^{-2}. The values of $\alpha'_{\mathbb{P}}$ and α'_{eff} are very sensitive to the gluon propagation radius R_c and can eventually be used to fix this poorly known parameter. At the moment we explore major properties of the solution for $R_c = 0.27$ fm.

One of interesting prediction from color dipole phenomenology of a diffraction cone is that the diffraction slope for the J/Ψ production at $Q^2 = 100$ GeV^2 nearly coincides with that for real photoproduction of the Υ. This is still another example of flavor symmetry restoration, because the scanning radii r_S for the two reactions are very close to each other.

The flavor symmetry properties of the diffraction cone can be seen in Fig. 10 (left box). The curves for $B(\gamma^* \to V)$ of all the vector mesons do converge together as a function of $Q^2 + m_V^2$, slight departures from exact flavor symmetry can be attributed to a difference of the

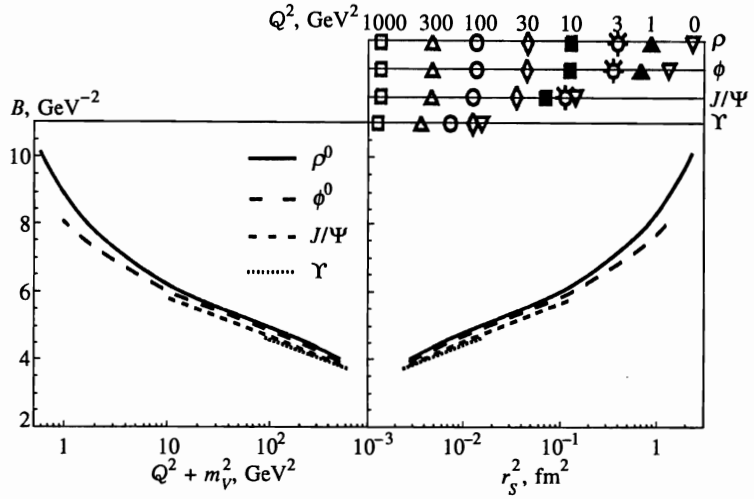

Fig. 10. The color dipole model predictions for the diffraction slope in production of different vector mesons as a function of the scaling variable $Q^2+m_V^2$ (left box) and the scanning radius r_S (right box) at fixed c.m.s. energy $W = 100$ GeV. The scales of Q^2 on the top of the right box show the values of Q^2 which correspond to the scanning radii shown on the bottom axis

pQCD scale factors $\tau(V)$ for light and heavy vector mesons. At fixed W, the calculated Q^2 dependence is an interplay of the changing scanning radius r_S and of the decrease of the Regge component with the increase of x_{eff}. For the light vector mesons and $Q^2 \lesssim 10$ GeV^2 the soft pomeron is substantial and the high precision experimental data on the ρ^0, ϕ^0 in this region of Q^2 are indispensable for better understanding of the soft pomeron. In Fig. 10 (right box) the same results are presented as a function of the scanning radius r_S as defined by Eq. (2) with $A = 6$. Crude estimates for the Q^2 dependence of $B(\gamma^* \to V)$ reported in [28] are close to the present results.

We can suggest useful empirical parameterizations for the diffraction slope. For production of heavy quarkonia, $V = J/\Psi, \Upsilon$, the Q^2 dependence of the diffraction slope at $W = 100$ GeV and in the considered range of $Q^2 \lesssim 500$ GeV^2 can be approximated by

$$B(\gamma^* \to V) \approx \beta_0 - \beta_1 \log \frac{Q^2 + m_V^2}{m_{J/\Psi}^2} \tag{64}$$

with the slope $\beta_1 \approx 1.1$ GeV^{-2} and the constant $\beta_0 \approx 5.8$ GeV^{-2}. Although (64) must be regarded only as a purely empirical crude parameterization, the logarithmic term (64) is suggestive of a substantial role of the term (50) in the diffraction slope at high energy. We recall that the constant β_0 is subject to the choice of the t range, it is a value of the slope β_1 which is more closely related to the gBFKL dynamics. For the light vector mesons, a somewhat better approximation to the results shown in Fig. 10 is

$$B(\gamma^* \to V) \approx \beta_0 - \beta_1 \log \left(\frac{Q^2 + m_V^2}{m_{J/\Psi}^2} \right) + \frac{\beta_2}{Q^2 + m_V^2} \tag{65}$$

with the same $\beta_1 = 1.1$ GeV^{-2} as above and with $\beta_0 = 7.1$ GeV^{-2}, $\beta_2 = 1.6$ for the ρ^0 production and $\beta_0 = 7.0$ GeV^{-2}, $\beta_2 = 1.1$ for the ϕ^0 production.

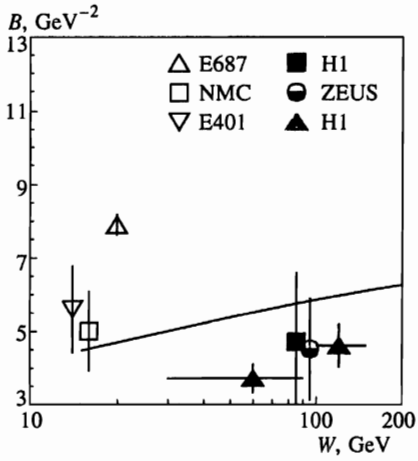

Fig. 11. Comparison of the color dipole model prediction for c.m.s. energy W dependence of the diffraction slope for photoproduction of the J/Ψ with the E401 [50], NMC [59], E687 [32], H1 [54, 55] and ZEUS [52, 53] data; $Q^2 = 0$

The experimental studies of the both Q^2 and energy dependence of the diffraction slope are in the formative stage. In the heavy quarkonium sector, only photoproduction of the J/Ψ has been studied to some extent. The experimental situation is summarized in Fig. 11, at the both fixed-target [32, 50, 59] and HERA energy [52–55] the error bars are too big for the definitive conclusions on the presence and/or lack of the shrinkage of the diffraction cone to be drawn. On the experimental side, the determinations of the diffraction slope are very sensitive to the rejection of the inelastic background. Only the E401 experiment [50] has used a technique which allowed a direct selection of the purely elastic events. The E401 result $B(W = 15\ \text{GeV}, Q^2 = 0) = 5.6 \pm 1.2\ \text{GeV}^{-2}$ is consistent with the NMC result $B(W = 15\ \text{GeV}, Q^2 = 0) = 5.0 \pm 1.1\ \text{GeV}^{-2}$ [59]. The recent high statistics Fermilab E687 experiment [32] has used the nuclear target and its determination of the diffraction slope for the quasielastic scattering, $B(W = 20\ \text{GeV}, Q^2 = 0) = 7.99 \pm 0.23\ \text{GeV}^{-2}$, is subject to the model-dependent separation of the coherent and quasielastic production on nuclei. At HERA, the first H1 data gave $B(W = 90\ \text{GeV}, Q^2 = 0) = 4.7 \pm 1.9\ \text{GeV}^{-2}$ [54] and the first ZEUS data gave $B(W = 90\ \text{GeV}, Q^2 = 0) = 4.5 \pm 1.4\ \text{GeV}^{-2}$ [52], updated with higher statistics to $B(W = 90\ \text{GeV}, Q^2 = 0) = 4.6 \pm 0.6\ \text{GeV}^{-2}$ [53]. In 1996 the H1 collaboration [55] found weak evidence for shrinkage of the diffraction cone: $B(W \sim 60\ \text{GeV}, Q^2 = 0) = 3.7 \pm 0.2 \pm 0.2\ \text{GeV}^{-2}$ and $B(W \sim 120\ \text{GeV}, Q^2 = 0) = 4.6 \pm 0.3 \pm 0.3\ \text{GeV}^{-2}$.

For virtual production of J/Ψ the H1 collaboration [58] reported in 1996 the first data:

$$B(W = 90\ \text{GeV}, \langle Q^2 \rangle = 18\ \text{GeV}^2) = 3.8 \pm 1.2(\text{stat.})^{+2.0}_{-1.6}(\text{syst.})\ \text{GeV}^{-2}.$$

Recently the ZEUS collaboration [57] presented the value of the diffraction slope at $Q^2 = 6\ \text{GeV}^2$:

$$B(W = 90\ \text{GeV}, \langle Q^2 \rangle = 6\ \text{GeV}^2) = 4.5 \pm 0.8(\text{stat.}) \pm 1.0(\text{syst.})\ \text{GeV}^{-2}.$$

We predict the decrease of the diffraction slope from $Q^2 = 0$ to $Q^2 = 18\ \text{GeV}^2$ by mere $\approx 0.5\ \text{GeV}^{-2}$, too small an effect to be seen at the present experimental accuracy.

The end-point contribution from asymmetric large size dipoles with $z(1 - z) \ll 1$ is different for the production of the T and L polarized vector mesons and makes the average scanning radius somewhat larger in the case of the T polarization. Consequently, one would

expect the inequality of diffraction slopes, $B_T > B_L$, for the polarization states. But the numerical difference between them is negligible even for the charmonium states, because in the nonrelativistic quarkonium the end-point effects are strongly suppressed. For the bottonium states the $B_T - B_L$ is absolutely negligible.

9. WHAT IS SPECIAL ABOUT DIFFRACTIVE PRODUCTION OF THE RADIALLY EXCITED STATES $V(2S)$?

In the diffraction production of radially excited $2S$ states (Ψ', Υ') the keyword is the node effect. The radial wave function of the $2S$ state changes the sign at $r \sim R_V(1S)$ and there are cancelations of contributions to the production amplitude from large dipoles, $r \gtrsim R_V(1S)$, and small dipoles, $r \lesssim R_V(1S)$, which were noticed for the first time in [1, 3]. Manifestations of the node effect for diffractive production of light vector mesons off nuclei have been discussed in [30, 60]. The detailed analysis of the forward real and virtual photoproduction of light $2S$ states (ρ', ϕ') at high energies is presented in [10]. The major subject of the present discussion is new manifestations of the node for the diffraction cone.

The cancellation pattern obviously depends on the relationship between r_S and position of the node r_n which is close to the radius of the $1S$ state, $r_n \sim R_V(1S)$. If $r_S \ll R_V(1S)$, then the wrong-sign contribution to the production amplitudes from dipoles with $r \gtrsim r_n$ is small and cancelations are weak (the undercompensation scenario of Ref. 30). If $r_S \gtrsim R_V(1S)$, then the production amplitude can even be dominated by the wrong-sign contribution from r above the node position (the overcompensation scenario). For the heavy quarkonia the scanning radius r_S is sufficiently small even at $Q^2 = 0$, and the undercompensation scenario is realized.

At fixed target energies, the node effect is sufficiently strong and suppresses the ratio $R_{21}(t = 0) = [d\sigma(\Psi')/d\sigma(J/\Psi)]_{t=0}$ by almost one order in magnitude (Fig. 12). Evidently, the smaller is the scanning radius the smaller is the large-r contribution and the weaker is the node effect, so that the ratio $[d\sigma(\Psi')/d\sigma(J/\Psi)]_{t=0}$ rises with Q^2 as shown in Fig. 12. When the node effect is strong which is the case for the Ψ' at $Q^2 = 0$, then even slight variations of the scanning radius r_S can change the strength of the node effect substantially. For this reason one must not be surprised that at fixed target energies the ratio $[d\sigma(\Psi')/d\sigma(J/\Psi)]_{t=0}$ changes with Q^2 quite rapidly, on a scale of Q^2 smaller than the natural scale m_V^2. The predicted energy dependence of $[d\sigma(\Psi')/d\sigma(J/\Psi)]_{t=0}$ derives from the faster growth with energy of the dipole

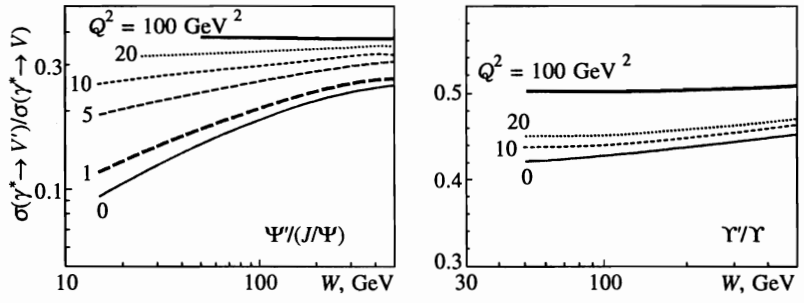

Fig. 12. The color dipole model predictions for the Q^2 and W dependence of the ratios $d\sigma(\gamma^* \to \Psi'(2S))/d\sigma(\gamma^* \to J/\Psi)$ and $d\sigma(\gamma^* \to \Upsilon'(2S))/d\sigma(\gamma^* \to \Upsilon)$ for the polarization-unseparated forward differential cross sections

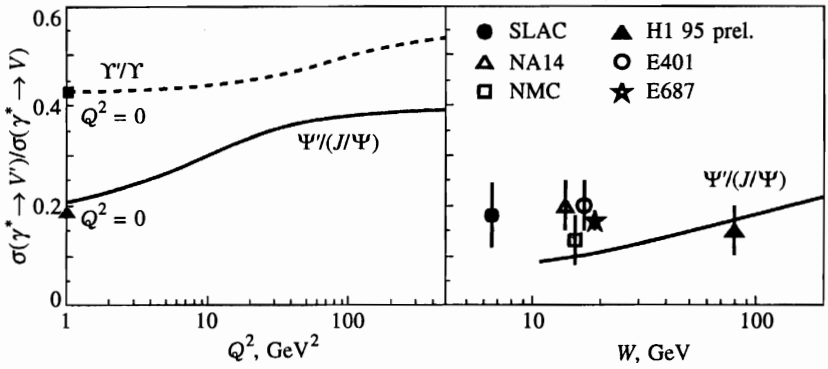

Fig. 13. The left box shows the color dipole model predictions for the Q^2 dependence of the ratio of the t-integrated polarization-unseparated cross sections $\sigma(\gamma^* \to \Psi'(2S))/\sigma(\gamma^* \to J/\Psi)$ and $\sigma(\gamma^* \to \Upsilon'(2S))/\sigma(\gamma^* \to \Upsilon)$ at c.m.s. energy $W = 100$ GeV. The right box shows comparison of the color dipole model prediction for c.m.s. energy W dependence of the ratio $\sigma(\gamma \to \Psi')/\sigma(\gamma \to J/\Psi)$ at $Q^2 = 0$ with the E401 [50], NMC [31], E687 [32], NA14 [62], SLAC [63] and H1 [33] data

cross section for smaller dipoles which also diminishes the node effect. In Fig. 13 (left box) we show in more detail for the HERA energy $W = 100$ GeV the Q^2 dependence of the ratio of the t-integrated cross sections $\sigma(2S)/\sigma(1S)$ evaluated using the diffraction slope $B(2S)$ described below. The both predicted Q^2 and W dependences of the node effect are sufficiently strong to be observed at HERA. Because for the heavier b quarks the scanning radius in comparison to $R_V(1S)$ is substantially smaller than for the charmed quarks, the node effect in the bottonium production is much weaker, the ratio $[d\sigma(\Upsilon')/d\sigma(\Upsilon)]_{t=0}$ is larger and exhibits much weaker Q^2 and W dependences than for the charmonium states (Fig. 12).

The node effect is slightly different for the T and L polarizations. This is best seen in Fig. 5 which shows that the ratio $R_{LT}(2S)$ for the $V'(2S)$ production which is different from $R_{LT}(1S)$ both in the magnitude and Q^2, W dependence.

The new effect which we focus here on is a nontrivial impact of the node effect on the diffraction cone. In the conventional situation the larger are the radii of the participating particles the larger is the diffraction slope and for real photoproduction we have a clear hierarchy

$$B(\gamma \to \rho^0) > B(\gamma \to \phi^0) > B(\gamma \to J/\Psi) > B(\gamma \to \Upsilon) \tag{66}$$

which follows the hierarchy of radii $R_{\rho^0} > R_{\phi^0} > R_{J/\Psi} > R_\Upsilon$. Although the mean squared radius of the Ψ' is about twice as large than $R_{J/\Psi}$,, the color dipole approach uniquely predict $B(\gamma \to \Psi') < B(\gamma \to J/\Psi)$ in a striking defiance of the hierarchy (66), which has the following origin: let $\mathcal{M}_<$ and $\mathcal{M}_>$ be the moduli of contributions to the $V(2S)$ production amplitude from color dipoles with size r below and above the position of the node in the $2S$ radial wave function and let $B_<$ and $B_>$ be the diffraction slopes for the corresponding contributions. Because of the hierarchy (66) we have a strong inequality

$$B_> > B_< . \tag{67}$$

For production of the $V(1S)$ state $B(1S) \approx B_<$. Now, the total $V(2S)$ production amplitude equals $\mathcal{M}(2S) = \mathcal{M}_< - \mathcal{M}_>$, and for the diffraction slope we find

$$B(2S) = \frac{B_< \mathcal{M}_< - B_> \mathcal{M}_>}{\mathcal{M}_< - \mathcal{M}_>} = B_< - (B_> - B_<)\frac{\mathcal{M}_>}{\mathcal{M}_< - \mathcal{M}_>}, \tag{68}$$

which gives an estimate

$$B(2S) - B(1S) \approx -(B_> - B_<)\frac{\mathcal{M}_>}{\mathcal{M}_< - \mathcal{M}_>} < 0. \tag{69}$$

The weaker is the node effect the smaller is the difference of diffraction slopes $B(2S) - B(1S)$. The typical color dipole sizes r which enter $M_<$ and $M_>$ differ by $\sim R_V(1S)$, and the difference of slopes $B_> - B_<$ can be evaluated as a variation of the diffraction slope $B(1S)$ when the scanning radius r_S changes by the factor ~ 2 from its value at $Q^2 = 0$. Then the parameterization gives for heavy quarkonia an estimate $B_> - B_< \sim (1\text{–}2)\beta_1 \sim 1$ GeV^{-2}. Equation (69) shows that the splitting $B(2S) - B(1S)$ is further suppressed if the node effect is weak, i.e., if $\mathcal{M}_> \ll \mathcal{M}_<$.

The results for the $B(1S) - B(2S)$ are presented in Fig. 14. For the bottonium family the node effect is negligibly weak, cf. Fig. 12, whereas for the charmonium family the chances of the experimental observation of the inequality $B(2S) < B(1S)$ are not nil at least in real photoproduction and in the fixed-target experiments. The difference of diffraction slopes $B(1S) - B(2S)$ is larger for the L polarization conforming to a stronger node effect for L polarization. As discussed above and shown in Fig. 12, the node effect diminishes with energy and the difference of diffraction slopes $B(1S) - B(2S)$ drops by the factor ~ 2 from the fixed-target energy to HERA energy. It vanishes at large Q^2 following the demise of the node effect in Fig. 12, the remarks on the rapid variation of the node effect on a scale of Q^2 smaller than m_V^2 at fixed-target energies $W \sim 15$ GeV are fully relevant to $B(1S) - B(2S)$ too.

Another demonstration of the node effect leading to inequality $B(2S) < B(1S)$ is presented in Fig. 15 in the form of the t dependence of the differential cross section ratio

$$R_{V'/V}(t) = \frac{d\sigma(\gamma \to V')/dt}{d\sigma(\gamma \to V)/dt} \tag{70}$$

for real photoproduction. The ratio $R_{\Psi'/(J/\Psi)}(t)$ rises with t at $W = 15$ GeV as a consequence of the node effect, whereas at $W = 100$ GeV Fig. 15 shows practically constant t dependence

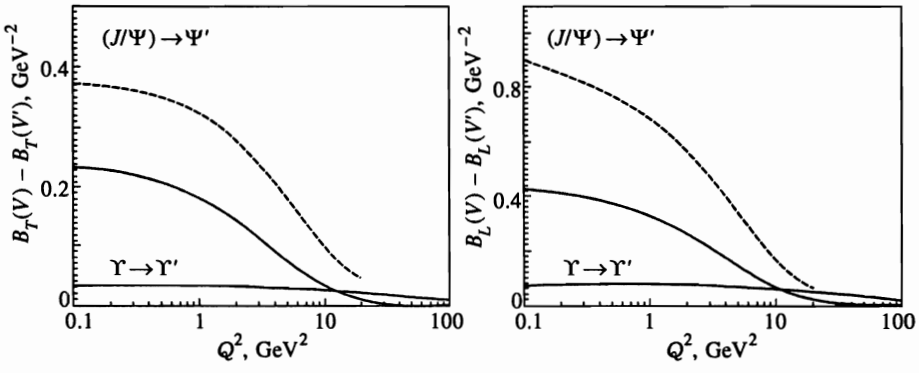

Fig. 14. The color dipole model predictions for the difference of diffraction slopes $B(1S) - B(2S)$ vs. Q^2 at c.m.s. energy $W = 15$ GeV (dashed lines) and $W = 100$ GeV (solid lines) for T and L polarization

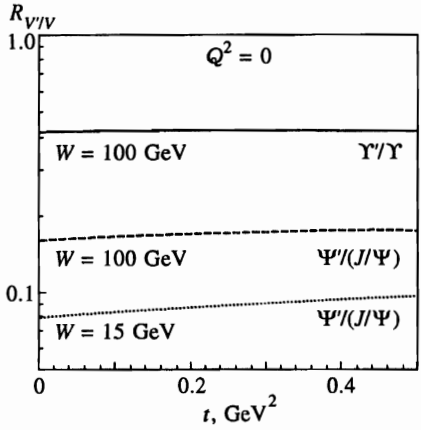

Fig. 15. The color dipole model predictions for t dependence of the ratio differential cross section $R_{V'/V}(t)$ given by (70) for the $\Psi'/(J/\Psi)$ and Υ'/Υ real photoproduction

of $R_{\Psi'/(J/\Psi)}(t)$ and $R_{\Upsilon'/\Upsilon}(t)$ corresponding to a weaker node effect at larger energy and for heavier vector mesons, respectively, see also Fig. 14.

There is a solid experimental evidence for the node effect in real photoproduction of the Ψ'. In 1996 the H1 collaboration reported the first observation of real photoproduction of the Ψ' at HERA with the result $R_{21} = \sigma(\gamma \to \Psi')/\sigma(\gamma \to J/\psi) = 0.15 \pm 0.05$ [33]. Concerning the fixed target experiments, only E401 has used the hydrogen target with the result $\sigma(\gamma \to \Psi')/\sigma(\gamma \to J/\psi) = 0.20 \pm 0.05$ at $W = 17$ GeV. Nuclear targets have been used in all other experiments. Evaluation of the cross section ratio for the hydrogen target from these data requires corrections for the nuclear shadowing of the J/Ψ production and nuclear antishadowing of the Ψ' production, there are also systematic uncertainties with the separation of coherent and incoherent production. Specifically, within the same color dipole model as used in this paper it has been shown [1] that the ratio $R_{21} = \sigma(\gamma \to \Psi')/\sigma(\gamma \to J/\psi)$ is enhanced in incoherent production off nuclei by the factor 1.26, 1.55, and 2.16 for the Be, Fe, and Pb nuclei, respectively. For the relatively dilute ^{6}Li target the enhancement factor can be estimated as ≈ 1.1. Then, the E687 result $R_{21}(\text{E687}) = 0.21 \pm 0.02$ for the Be target at $W = 19$ GeV [32] corresponds to $R_{21}(\text{E687}; N) = 0.17 \pm 0.02$ for the free nucleon target, the NMC result $R_{21} = 0.20 \pm 0.05(\text{stat.}) \pm 0.07(\text{syst.})$ [31] after correction for the last value [61] of the branching ratio $BR(J/\Psi \to \mu^+\mu^-) = 5.97 \pm 0.25\%$ gives $R_{21} = 0.17 \pm 0.04(\text{stat.}) \pm 0.04(\text{syst.})$ for the passive concrete absorber at $W = 15$ GeV which corresponds to $R_{21}(\text{NMC}; N) = 0.13 \pm 0.05$ for the free nucleon target. The NA14 result 0.22 ± 0.05 for the Li target at $W = 14$ GeV [62] corresponds to $R_{21}(\text{NA14}; N) = 0.2 \pm 0.05$ for the free nucleon target and the SLAC result 0.22 ± 0.08 for the Be target at $W \simeq 6.5$ GeV [63] corresponds to $R_{21}(\text{SLAC}; N) = 0.18 \pm 0.07$ for the free nucleon target. In Fig. 13 (right box) we compare our prediction for $R_{21}(N) = \sigma(\gamma \to \Psi')/\sigma(\gamma \to J/\psi)$ for real photoproduction on protons with the H1 and E401 data for the proton target and the above evaluations of $R_{21}(N)$ from the nuclear-target data. The overall agreement between the theory and experiment is satisfactory. In view of the steady collection of the data at HERA, the higher precision fixed-target data on the hydrogen target are highly desirable to check unambiguously the predicted rise of $R_{21}(N)$ with energy.

10. THE SUMMARY AND CONCLUSIONS

The major focus of this work has been on the forward cone for diffractive real and virtual photoproduction of ground ($1S$) and radially excited ($2S$) states of heavy quarkonia in the framework of color dipole running gBFKL approach. We presented a detailed discussion of the color dipole factorization for diffractive amplitudes and of the relevant pQCD factorization scales with a strong emphasis on restoration of the flavor symmetry in the variable $Q^2+m_V^2$. We based our analysis on solutions of the gBFKL equations for the dipole cross section [26, 5] and for the diffraction slope for the color dipole scattering amplitude [28]. Starting from the same dipole cross section which provides a good quantitative description of the rise of the proton structure function at small x [26, 27], we found encouraging agreement with the experimental data on the Q^2 and energy dependence of diffractive J/Ψ production. There are many interesting predictions for the J/Ψ production to be tested, for instance, the Q^2 dependence of the effective intercept Δ_{eff}.

A detailed analysis of the energy and Q^2 dependence of the diffraction slope $B(\gamma^* \to V)$ for vector meson production is presented here for the first time. Of primary interest is the shrinkage of the diffraction cone which follows from the finding [28] that the gBFKL pomeron is a set of moving poles. We identified different sources of the Q^2 dependence of the diffraction slope. Based on the solution [28] of the running gBFKL equation for the diffraction slope, we presented detailed calculations of the Q^2 and W dependence of $B(\gamma^* \to V)$. The present experimental data on $B(\gamma^* \to V)$ for the J/Ψ production are not yet accurate enough to rule in or rule out our predictions for the shrinkage of the diffraction cone.

Diffractive production of the radially $2S$ mesons (Ψ', Υ') is a subject on its own. The key new feature of production of the $2S$ states is the node effect, the destructive interference of contributions to production amplitude from small and large color dipoles because of the node in the radial wave function of $2S$ radial excitations. The resulting strong suppression of the Ψ' photoproduction agrees with the available experimental data. An interesting prediction from the color dipole dynamics to be tested is a rise of the cross section ratio $\sigma(\gamma \to \Psi')/\sigma(\gamma \to J/\Psi)$ by the factor two from the CERN-FNAL to HERA energies. The new consequence of the node effect which we discussed in this paper is a counterintuitive inequality of diffraction slopes, $B(\gamma \to \Psi') < B(\gamma \to J/\Psi)$, to be contrasted to a familiar rise of the diffraction slope for elastic scattering processes with the rise of the radius of the beam and target particles. The scanning phenomenon allows one to control the node effect varying the scanning radius with Q^2 and we present the corresponding predictions for the Q^2 dependence of the cross section ratio $\sigma(\gamma \to \Psi')/\sigma(\gamma \to J/\Psi)$ and of the difference of diffraction slopes $B(\gamma \to \Psi') - B(\gamma \to J/\Psi)$. The predicted effects for the charmonium family are within the reach of modern experiments. The present analysis of diffractive production of heavy mesons provides a useful benchmark for future applications to light vector mesons. The experimental comparison of virtual and real photoproduction of vector mesons will shed light on the transition between the soft pomeron exchange which dominates for the ρ^0, ω^0, ϕ^0 production at small and moderate Q^2 to the gBKFL pomeron exchange at higher Q^2 and/or heavy vector mesons.

This work was partly supported by the INTAS grant 93-0239ext. B. G. Z. and V. R. Z. thank Prof. J. Speth for hospitality at IKP, Jülich, where this work has partly been carried out.

References

1. B. Z. Kopeliovich and B. G. Zakharov, Phys. Rev. D **44**, 3466 (1991).
2. M. G. Ryskin, Z. Phys. C **57**, 89 (1993).
3. N. N. Nikolaev, Comments on Nucl. Part. Phys. **21**, 41 (1992); B. Z. Kopeliovich, J. Nemchik, N. N. Nikolaev, and B. G. Zakharov, Phys. Lett. B **309**, 179 (1993).
4. B. Z. Kopeliovich, J. Nemchik, N. N. Nikolaev, and B. G. Zakharov, Phys. Lett. B **324**, 469 (1994).
5. J. Nemchik, N. N. Nikolaev, and B. G. Zakharov, Phys. Lett. B **341**, 228 (1994).
6. S. J. Brodsky, L. L. Frankfurt, J. F. Gunion, A. H. Mueller, and M. Strikman, Phys. Rev. D **50**, 3134 (1994).
7. J. R. Forshaw and M. G. Ryskin, Phys. Lett. B **375**, 301 (1996).
8. D. Yu. Ivanov, Phys. Rev. D **53**, 3564 (1996); I. F. Ginzburg and D. Yu. Ivanov, Phys. Rev. D **54**, 5523 (1996).
9. J. Nemchik, N. N. Nikolaev, E. Predazzi, and B. G. Zakharov, Phys. Lett. B **374**,199 (1996).
10. J. Nemchik, N. N. Nikolaev, E. Predazzi, and B. G. Zakharov, Z. Phys. C **75**, 71 (1997).
11. H. G. Dosch, T. Gousset, G. Kulzinger, and H. J. Pirner, Phys. Rev. D **55**, 2602 (1997).
12. E. A. Kuraev, L. N. Lipatov, and S. V. Fadin, Sov. Phys. JETP **44**, 443 (1976); **45**, 199 (1977); I. Balitsky and L. N. Lipatov, Sov. J. Nucl. Phys. **28**, 822 (1978).
13. L. N. Lipatov, Sov. Phys. JETP **63**, 904 (1986) 904; L. N. Lipatov, in *Perturbative Quantum Chromodynamics*, ed. by A. H. Mueller, World Scientific (1989), p. 411.
14. N. Nikolaev and B. G. Zakharov, JETP **78**, 598 (1994); Z. Phys. C **64**, 631 (1994).
15. N. N. Nikolaev, B. G. Zakharov, and V. R. Zoller, JETP Lett. **59**, 6 (1994); JETP **78**, 866 (1994); Phys. Lett. B **328**, 486 (1994).
16. V. N. Gribov and L. N. Lipatov, Sov. J. Nucl. Phys. **15**, 438 (1972); L. N. Lipatov, Sov. J. Nucl. Phys. **20**, 181 (1974); Yu. L. Dokshitser, Sov. Phys. JETP **46**, 641 (1977); G. Altarelli and G. Parisi, Nucl. Phys. B **126**, 298 (1977).
17. N. N. Nikolaev and B. G. Zakharov, Phys. Lett. B **327**, 157 (1994).
18. E. M. Levin, Nucl. Phys. B **453**, 303 (1995).
19. K. D. Anderson, D. A. Ross, and M. G. Sotiropoulos, preprint SHEP-97-09 and UM-TH-97-12 (1997), hep-ph/9705466.
20. E. Schuryak, Rev. Mod. Phys. **65**, 1 (1993).
21. E. Gotsman and S. Nussinov, Phys. Rev. D **22**, 624 (1980).
22. A. B. Migdal, JETP Lett. **46**, 256 (1987).
23. A. H. Mueller, Nucl. Phys. B **415**, 373 (1994).
24. N. N. Nikolaev and B. G. Zakharov, Z. Phys. C **49**, 607 (1991) 607; Z. Phys. C **53**, 331 (1992).
25. V. Barone, M. Genovese, N. N. Nikolaev, E. Predazzi, and B. G. Zakharov, Phys. Lett. B **326**, 161 (1994).
26. N. N. Nikolaev and B. G. Zakharov, Phys. Lett. B **327**, 149 (1994).
27. N. N. Nikolaev, B. G. Zakharov, and V. R. Zoller, Pis'ma Zh. Eksp. Teor. Fiz. **66**, 134 (1997) [JETP Lett. **66**, 138 (1997)].
28. N. N. Nikolaev, B. G. Zakharov, and V. R. Zoller, Phys. Lett. B **366**, 337 (1996).
29. N. N. Nikolaev, B. G. Zakharov, and V. R. Zoller, JETP Lett. **60**, 694 (1994).
30. J. Nemchik, N. N. Nikolaev, and B. G. Zakharov, Phys. Lett. B **339**, 194 (1994).
31. NMC Collab.: P. Amaudruz, M. Arneodo, A. Arvidson et al., Nucl. Phys. B **371**, 553 (1992).
32. P. Frabetti, V. S. Paolone, P. M. Yager et al., presented on Int. Europhys. Conf. on HEP, Brussels, July 27–August 2, 1995.
33. H1 Collab.: C. Adloff, S. Aid, M. Anderson et al., preprint DESY 97-228 (1997), hep-ex/9711012.
34. V. N. Gribov, Sov. Phys. JETP **30**, 709 (1970).
35. G. Veneziano, Phys. Lett. B **52**, 220 (1974); Nucl. Phys. B **74**, 365 (1974); S. Nussinov, Phys. Rev. Lett. **34**, 1286 (1975); G. F. Chew and C. Rosenzweig, Phys. Rep. **41**, 264 (1978); A. Cappela and J. Tran Thanh Van, Phys. Lett. B **114**, 450 (1982).

36. P. V. Landshoff and O. Nachtmann, Z. Phys. C **35**, 405 (1987).
37. A. Donnachie and P. V. Landshoff, Phys. Lett. B **185**, 403 (1987); J. R. Cuddell, Nucl. Phys. B **336**, 1 (1990).
38. V. N. Gribov and A. A. Migdal, Sov. J. Nucl. Phys. **8**, 703 (1969).
39. N. N. Nikolaev and B. G. Zakharov, Phys. Lett. B **332**, 184 (1994).
40. S. Catani, M. Ciafaloni, and F. Hautmann, Nucl. Phys. B **366**, 135 (1991).
41. B. G. Zakharov, Sov. J. Nucl. Phys. **49**, 860 (1989); J. F. Gunion and D. F. Soper, Phys. Rev. D **15**, 2617 (1977).
42. V. Barone, M. Genovese, N. N. Nikolaev et al., Z. Phys. C **58**, 541 (1993).
43. M. Genovese, N. N. Nikolaev, and B. G. Zakharov, Zh. Exp. Teor. Fiz. **108**, 1141, 1155 (1995).
44. N. N. Nikolaev, W. Schaefer, and B. G. Zakharov, preprint KFA-IKP-TH-1996-06 (1996), hep-ph/9608338.
45. A. Schiz, L. A. Fajardo, R. Majka et al., Phys. Rev. D **24**, 26 (1981); J. P. Burq, M. Chemarin, M. Chevallier et al., Phys. Lett. B **109**, 111 (1982).
46. B. Z. Kopeliovich, N. N. Nikolaev, and I. K. Potashnikova, Phys. Rev. D **39**, 769 (1989).
47. N. N. Nikolaev and B. G. Zakharov, Phys. Lett. B **333**, 250 (1994).
48. EMC Collab.: J. J. Aubert, G. Bassompiere, K. H. Becks et al., Nucl. Phys. B **213**, 1 (1983); EMC Collab.: J. Ashman, B. Badelek, G. Baum et al., Z. Phys. C **39**, 169 (1988).
49. E516 Collab.: B. H. Denby, V. K. Bharadwai, D. J. Summers et al., Phys. Rev. Lett. **52**, 795 (1984).
50. E401 Collab.: M. Binkley, C. Bohler, J. Butler et al., Phys. Rev. Lett. **48**, 73 (1982).
51. E687 Collab.: P. L. Frabetti, V. S. Paolone, P. M. Yager et al., Phys. Lett. B **316**, 197 (1993).
52. ZEUS Collab.: M. Derrick, D. Krakauer, S. Magill et al., Phys. Lett. B **350**, 120 (1995).
53. ZEUS Collab.: J. Breitweg, M. Derrick, D. Krakauer et al., Z. Phys. C **75**, 215 (1997).
54. H1 Collab.: T. Ahmed, S. Aid, V. Andreev et al., Phys. Lett. B **338**, 507 (1994); H1 Collab.: S. Aid, V. Andreev, B. Andrieu et al., Nucl. Phys. B **472**, 3 (1996).
55. H1 Collab.: S. Aid, V. Andreev, B. Andrieu et al., *Diffractive and Non-Diffractive Photoproduction of J/Ψ at H1*, paper pa02-085, submitted to the 28th Intern. Conf. on High Energy Physics, Warsaw, Poland, 25–31 July 1996.
56. H1 Collab.: C. Adloff, S. Aid, M. Anderson et al., *Elastic Production of J/Ψ Mesons in Photoproduction and at High Q^2 at HERA*, paper № 242, submitted to the Intern. Europhys. Conf. on High Energy Physics, HEP97, Jerusalem, Israel, August 1997.
57. ZEUS Collab.: J. Breitweg, M. Derrick, D. Krakauer et al., *Exclusive Vector Meson Production in DIS at HERA*, paper № 639, submitted to the Intern. Europhys. Conf. on High Energy Physics, HEP97, Jerusalem, Israel, August, 1997.
58. H1 Collab.: S. Aid, V. Andreev, B. Andrieu et al., Nucl. Phys. B **468**, 3 (1996).
59. NMC Collab.: M. Arneodo, A. Arvidson, B. Badelek et al., Phys. Lett. B **332**, 195 (1994).
60. O. Benhar, B. G. Zakharov, N. N. Nikolaev et al., Phys. Rev. Lett. **74**, 3565 (1995); O. Benhar, S. Fantoni, N. N. Nikolaev et al., Zh. Exp. Teor. Fiz. **111**, 769 (1997).
61. *Review of Particle Properties*, Phys. Rev. D **50**, 1177 (1994).
62. NA14 Collab.: R. Barate, P. Bareyre, D. Bloch et al., Z. Phys. C **33**, 505 (1987).
63. SLAC Collab.: U. Camerini, J. G. Learned, R. Prepost et al., Phys. Rev. Lett. **35**, 483 (1975).